



Mechanistic investigations of the formation of multifunctional products from the multi-generation $\cdot\text{OH}$ oxidation of styrene

Long Chen^{1,2,3}, Yu Huang^{1,2,3}, Yonggang Xue^{1,2,3}, Long Cui^{1,2,3}, and Zhihui Jia⁴

¹State Key Laboratory of Loess Science, Institute of Earth Environment,
Chinese Academy of Sciences, Xi'an, 710061, China

²National Observation and Research Station of Regional Ecological Environment Change and Comprehensive
Management in the Guanzhong Plain, Xi'an, 710061, China

³Shaanxi Key Laboratory of Atmospheric and Haze-fog Pollution Prevention, Xi'an, 710061, China

⁴School of Materials Science and Engineering, Shaanxi Normal University, Xi'an, Shaanxi, 710119, China

Correspondence: Yu Huang (huangyu@ieecas.cn)

Received: 22 September 2025 – Discussion started: 23 October 2025

Revised: 24 March 2026 – Accepted: 25 March 2026 – Published: 13 April 2026

Abstract. Styrene is a highly reactive aromatic hydrocarbon that has been identified as a key secondary organic aerosol (SOA) precursor. Recent laboratory chamber experiments have identified C_7 and C_8 series compounds as the main components of SOA in the photooxidation of styrene. However, their molecular structures and formation pathways remain largely uncharacterized. Herein, the formation mechanisms of multifunctional products from the multi-generation $\cdot\text{OH}$ oxidation of styrene are studied using the quantum chemistry methods. The calculations show that the first generation RO_2 radicals can either proceed unimolecular decomposition to yield benzaldehyde ($\text{C}_7\text{H}_6\text{O}$), or undergo bimolecular reactions with $\text{HO}_2\cdot/\text{NO}$ to form the first generation closed-shell C_7 - and C_8 -products, hydroperoxide 1st- ROOH ($\text{C}_8\text{H}_{10}\text{O}_3$), benzaldehyde, and organic nitrate 1st- RONO_2 ($\text{C}_8\text{H}_9\text{NO}_3$). For the second generation $\cdot\text{OH}$ oxidation, OH-addition reaction occurring at the *ortho*-site of 1st- ROOH and 1st- RONO_2 has a significant dominance. The *ortho*-OH-addition products can proceed through two O_2 -addition steps and a cyclization process to produce the peroxide bicyclic peroxy radicals (BPR). BPR can further react with $\text{HO}_2\cdot/\text{NO}$ to form the second generation closed-shell C_8 -products, hydroperoxide 2nd- ROOH ($\text{C}_8\text{H}_{12}\text{O}_8$), organic nitrate 2nd- RONO_2 ($\text{C}_8\text{H}_{10}\text{N}_2\text{O}_{10}$), and other multifunctional products, in which the first two products have fractional yields of 41.4 % and 4.8 %, respectively. For the third generation $\cdot\text{OH}$ oxidation, OH-addition occurring at the $\text{C}=\text{C}$ double bond of 2nd- ROOH and 2nd- RONO_2 has the lowest barrier. The major third generation closed-shell C_8 -products are the multifunctional hydroperoxides and organic nitrates. These findings carry important implications for advancing our understanding of the chemical composition and formation mechanisms of aromatic SOA.

1 Introduction

Aromatic compounds are recognized as the significant secondary organic aerosol (SOA) precursors, accounting for 20 %–30 % of the total volatile organic compounds (VOCs) and up to ~ 60 % of the urban atmosphere (Xu et al., 2020; Yan et al., 2019; Yu et al., 2022a, b; Cabrera-Perez et al., 2016; Iyer et al., 2023; Wang et al., 2017; Bloss et al.,

2005; Forstner et al., 1997). The primary sources include the incomplete combustion, solvent evaporation, and industrial emission, and the secondary sources involve the biofuel and biomass burning (Xu et al., 2020; Cabrera-Perez et al., 2016; Li et al., 2019). The most abundant aromatic compounds, including benzene, toluene, ethylbenzene, xylenes, styrene and trimethylbenzenes, are highly present in urban environments (Cabrera-Perez et al., 2016; Koppmann, 2008). The degra-

dation of aromatic compounds initiated by the atmospheric oxidants (e.g., OH radicals, NO₃ radicals, O₃, and Cl atom) leads to the production of multifunctional molecules (e.g., nitroaromatics, dicarbonyls, cresols, epoxides) (Ji et al., 2017; Wu et al., 2014; Fu et al., 2023; Wang and Li, 2021; Wang et al., 2013, 2020b; Zaytsev et al., 2019), significantly contributing to new particle formation (NPF) and SOA formation (up to 50 % in eastern China) in the atmosphere (Wang et al., 2017, 2020a; Garmash et al., 2020; Molteni et al., 2018; Nie et al., 2022).

The secondary organic aerosol formation potential (SOAP) of aromatics is significantly greater than that of alkanes and alkenes during haze episodes in Beijing (Sun et al., 2016). Among these precursors, toluene is the predominant SOA-forming species, contributing more than 16 % of the total SOA, followed by styrene (15 %) and ethylbenzene (9.5 %) (Sun et al., 2016). Styrene is primarily emitted from the anthropogenic activities such as solvent usage and vehicle exhaust (Cho et al., 2014; Wu et al., 2021), which is detected at the ppb levels in urban environments, with the mixing ratios of 0.06–4.50 ppb (Cho et al., 2014; Huang et al., 2019). Styrene has been classified as a hazardous air pollutant in the 1990 Clean Air Act due to the potential mutagen and carcinogen (Environmental Protection Agency (EPA), 1990). Therefore, it is very necessary to investigate the degradation mechanisms of styrene under atmospheric conditions. In general, the atmospheric oxidation of styrene initiated by OH radicals is anticipated to be the dominant daytime sink, and the lifetime is estimated to be ~ 8 h under the conditions of typical OH radicals concentrations ($[\bullet\text{OH}] = \sim 2 \times 10^6 \text{ molec. cm}^{-3}$) (Wu et al., 2021; Shen et al., 2022). Due to the existence of highly reactive vinyl and aromatic groups, OH-initiated oxidation of styrene mainly comprise two kinds of pathways: H-abstraction and OH-addition, in which C _{β} -site OH-addition reaction is expected to be the predominant pathway (Wu et al., 2021; Wang et al., 2015; Zhang et al., 2024). The formed products can combine with an O₂ molecule leading to the first generation peroxy radicals, which can further react with NO resulting in the formation of benzaldehyde and formaldehyde. The barrier of the rate-limiting step is predicted to be 28.4 kcal mol⁻¹ (Wang et al., 2015), implying that benzaldehyde is unlikely to be the sole primary product in the oxidation of styrene due to their higher barriers. Additionally, carbonyl oxides, formed in the ozonolysis of styrene, serve as the chain units participating in the formation of oligomers (Yu et al., 2022a). The volatility of oligomers decreases dramatically as the successive addition of carbonyl oxides increases, eventually transforming into extremely low volatility organic compounds (ELVOC) and directly participating in NPF.

Experimentally, Cho et al., investigated the kinetics of the reaction styrene + $\bullet\text{OH}$ at 240–340 K and 1–3 Torr using the mass spectrometry technique (Cho et al., 2014). They found that the addition of OH radicals to the vinyl carbons is dominant, and the determined rate coefficient is $(5.80 \pm 0.49) \times$

$10^{-11} \text{ cm}^3 \text{ molec.}^{-1} \text{ s}^{-1}$ at room temperature. In the smog chamber experiments, Tajuelo et al. (2019a, b, c) found that the SOA yields from the photolysis and photooxidation of styrene and its homologous species increase with the concentration of initial reactants increasing, and benzaldehyde, benzoyl chloride, acetophenone and formaldehyde are expected to be the primary gas phase products. Yu et al. (2022b) investigated the formation of SOA from styrene in an indoor chamber under different NO_x and RH conditions, and found the SOA yields decrease with increasing RH in both the H₂O₂ and NO_x systems. The C₇ and C₈ species are the main products in the H₂O₂ system, while organic nitrates are the major components in the NO_x system. Although the possible molecular formula and chemical composition of the oxidation products from the reaction styrene + $\bullet\text{OH}$ are given in the aforementioned studies, the specific molecular structures and formation pathways remain ambiguous. Additionally, to the best of our knowledge, the majority of studies mainly focus on the first generation $\bullet\text{OH}$ oxidation products to date, while the formation mechanisms of multifunctional products from the multi-generation $\bullet\text{OH}$ oxidation of styrene are still limited.

In the present study, the multi-generation $\bullet\text{OH}$ oxidation mechanisms of styrene in the presence of HO₂/ NO are investigated using the quantum chemistry methods. The calculated results arising from the first generation $\bullet\text{OH}$ oxidation reactions are presented herein for comparison with the available literatures to ascertain the reliability of the employed theoretical method. For the multi-generation $\bullet\text{OH}$ oxidation reactions of styrene, all the possible pathways, including H-abstraction, OH-addition, O₂-addition, cyclization, ring-opening, intramolecular H-shifts, C–C bond and O–O bond scission, and HO₂-elimination, are taken into account. Additionally, the saturated concentrations of the formed multifunctional products are estimated to identify the volatility classes.

2 Computational methods

2.1 Electronic structures and energy calculations

The electronic structures and energy calculations of all stationary points, including reactants (R), intermediates (IM), transition states (TS) and products (P), are performed using the Gaussian 16 program (Frisch et al., 2016). Geometric optimizations of all stationary points on the potential energy surfaces (PESs) are carried out at the M06-2X/6-31+g(d,p) level of theory, since it has reliable performance for describing the noncovalent interactions, thermochemical, and kinetics (Zhao and Truhlar, 2008). Harmonic vibrational frequencies are determined at the M06-2X/6-31+g(d,p) theoretical level to confirm the characteristics of all stationary points (a local minimum or a saddle point). The zero-point vibrational energy (ZPVE) is scaled by a factor of 0.967 (Alecu et al., 2010). Intrinsic reaction coordinate (IRC) calcula-

tions are carried out to ascertain the connection of the given TS between the designated local minima R and P (Fukui, 1981). Single point energy calculations are performed at the M06-2X/6-311++G(3df,3pd) level based on the M06-2X/6-31+g(d,p) optimized geometries.

In order to further evaluate the reliability of the computational method employed herein, the single point energies of all the stationary points involved in the initial addition of OH radicals to styrene and intramolecular H-shift reactions of the first generation peroxy radicals S2-1-x are recalculated using the DLPNO-CCSD(T)/aug-cc-pVTZ method performed using the Orca 6.1 program (Neese, 2025). As shown in Table S1 in the Supplement, the ΔE_a values obtained using the M06-2X/6-311++G(3df,3pd) method are consistent with those derived from the DLPNO-CCSD(T)/aug-cc-pVTZ method. The largest deviation and the average absolute deviation are 1.2 and 0.6 kcal mol⁻¹, respectively, indicating that the computational method employed in this study is reliable. Considering the computational cost, the M06-2X/6-311++G(3df,3pd) method is employed to investigate the formation mechanism of multifunctional products from the multi-generation •OH oxidation of styrene. The energy barrier (ΔE_a) and reaction energy (ΔE_r) are defined as the difference in energy between TS and IM, as well as between P and R.

2.2 Conformer research

RO₂ radicals formed from the addition of O₂ to the carbon-centered site of alkyl radicals R have multiple possible conformers due to the different orientations of O₂ attack (Chen et al., 2021; Fu et al., 2020; Møller et al., 2016, 2020). An initial structure of RO₂ radicals is optimized at the B3LYP/6-31+G(d) level and subsequently used as the starting geometry to perform the conformer search conducted using the Molclus program (Lu, 2024). The resulting structures are initially optimized at the B3LYP/6-31+G(d) level, as this method accurately predicts the relative energy ordering of different conformers (Møller et al., 2016, 2020). For the intramolecular H-shift reactions of RO₂ radicals, the lengths of the O–O, C–H and O–H bonds in the conformational sampling of TSs are constrained to retain the cyclic TS structure. All unique conformers of R, TS and P within 5.0 kcal mol⁻¹ with respect to the lowest energy conformer are further optimized at the M06-2X/6-31+g(d,p) level of theory. Then, the single point energy calculations are performed at the M06-2X/6-311++G(3df,3pd) level of theory. RO radicals formed by the bimolecular reactions of RO₂ radicals with HO₂ radicals and NO also have multiple conformers. In order to obtain the lowest energy conformer, a similar methodology is employed in the present study.

2.3 Kinetics calculations

The rate coefficients of unimolecular reactions, including intramolecular H-shifts, cyclization, HO₂-elimination, and C–C bond and C–O bond scissions, are calculated using the RRKM theory along with energy-grained master equation (RRKM-ME) (Holbrook et al., 1996). The rate coefficients of bimolecular reactions, involving H-abstraction and OH-addition, are determined using the traditional transition state theory (TST) (Fernández-Ramos et al., 2007). An asymmetric one-dimensional Eckart model (Eckart, 1930) is employed to consider the tunneling correction factors in the rate coefficient calculations based on RRKM-ME and TST. A single exponential down model in the RRKM-ME calculations is utilized to approximate the collision transfer ($\langle \Delta E \rangle_{\text{down}} = 200 \text{ cm}^{-1}$). The Lennard–Jones parameters of all intermediate species are estimated using the empirical formula as proposed by Gilbert and Smith (1990).

For the intramolecular H-shifts of RO₂ and RO radicals, the rate coefficients are computed using the multiconformer transition state theory (MC-TST) (Møller et al., 2016), which is expressed as Eq. (1) (Møller et al., 2016, 2020; Pasik et al., 2024):

$$k_{\text{MC-TST}} = \kappa \frac{k_{\text{B}} T}{h} \frac{\sum_i^{\text{TS conf.}} \exp\left(\frac{-\Delta E_i}{k_{\text{B}} T}\right) Q_{\text{TS},i}}{\sum_j^{\text{R conf.}} \exp\left(\frac{-\Delta E_j}{k_{\text{B}} T}\right) Q_{\text{R},j}} \exp\left(-\frac{E_{\text{TS}} - E_{\text{R}}}{k_{\text{B}} T}\right) \quad (1)$$

where κ is the Eckart tunneling coefficient, h is Planck's constant, k_{B} is Boltzmann's constant, and T is the absolute temperature (298.15 K). $Q_{\text{TS},i}$ and $Q_{\text{R},j}$ refer to the partition functions of the corresponding transition state i and reactant j conformers, respectively. ΔE_i and ΔE_j represent the relative electronic energies between the corresponding transition state i and reactant j conformers and the lowest energy conformers, respectively. E_{TS} and E_{R} stand for the electronic energies of the lowest energy transition state and reactant conformers, respectively. All kinetics calculations are carried out using the KiSTheP 2021 and MESMER 6.0 programs (Glowacki et al., 2012; Canneaux et al., 2013).

3 Results and discussion

3.1 First generation •OH oxidation mechanisms of styrene

Styrene is composed of a benzene ring and a vinyl group, and its oxidation initiated by OH radicals may proceed either on the vinyl group or on the benzene ring. Previous literature has demonstrated that the addition of OH radicals to terminal carbon (C_β-site) of a vinyl group in styrene is the dominant pathway, with the branching ratio of 88.2% (Wu et al., 2021). Therefore, the C_β-site OH-addition reaction is mainly considered in the present study. Figure 1 depicts that this reaction starts with the formation of a pre-reactive complex IM1, and then transforms into an alkyl radical S1-1 via transition state TS1 with a ΔE_a of 0.8 kcal mol⁻¹.

The rate coefficient of C_{β} -site OH-addition reaction is estimated to be $1.5 \times 10^{-11} \text{ cm}^3 \text{ molec.}^{-1} \text{ s}^{-1}$ at ambient temperature, which is approximately consistent with the experimental ($1.2\text{--}6.2 \times 10^{-11} \text{ cm}^3 \text{ molec.}^{-1} \text{ s}^{-1}$) and theoretical values ($1.7\text{--}2.0 \times 10^{-11} \text{ cm}^3 \text{ molec.}^{-1} \text{ s}^{-1}$) for the total rate coefficient of the reaction styrene + $\bullet\text{OH}$ (Wu et al., 2021; Zhang et al., 2024).

Due to the existence of resonance structures with radical character on the aromatic ring, the resulting S1-1 can readily isomerize into three other species, namely, S1-2, S1-3 and S1-4. The attack of an O_2 molecule on the C-center site of S1-1 leads to the formation of the first generation peroxy radicals S2-1-x ($\Delta E_r > -59.6 \text{ kcal mol}^{-1}$). The formed S2-1-x includes eight energetically similar conformers due to the different orientations of O_2 attack. In order to distinguish the different conformers, the subscript letter x is used in the present study. The energy ordering of different conformers follows an alphabetical sequence, in which letter a denotes the lowest energy conformer. The Boltzmann population of different conformers in S2-1-x is listed in Table S2 in the Supplement.

For the unimolecular decomposition reactions of S2-1-x, there are three kinds of pathways. One is the intramolecular H-shift reactions, where the hydrogen atom migrates from the $-\text{CH}_2$, $-\text{CH}$ and $-\text{OH}$ groups to the terminal oxygen atom of the $-\text{OO}$ group leading to various alkyl and alkoxy radicals. Among these competing H-shift reactions, the hydrogen atom at the $-\text{OH}$ group can be transferred via a six-membered ring transition state (1,5-H shift) to yield an alkoxy radical S3-1-a, which exhibits the lowest barrier ($\Delta E_a = 21.0 \text{ kcal mol}^{-1}$). The resulting S3-1-a can undergo the $C_{\alpha}\text{--}C_{\beta}$ bond cleavage to produce a formaldehyde and an alkyl radical S4-1-a ($\Delta E_a = 0.8 \text{ kcal mol}^{-1}$), followed by an OH radical release to form benzaldehyde ($\Delta E_a = 0.1 \text{ kcal mol}^{-1}$). The rate coefficients for the aforementioned three pathways are calculated to be 2.7×10^{-4} , 4.6×10^{10} and $7.2 \times 10^{10} \text{ s}^{-1}$, respectively. Based on the values of ΔE_a and the corresponding rate coefficients, it can be concluded that the 1,5-H shift reaction is the rate-determining step in the formation of benzaldehyde. The other is the cyclization, where the $-\text{OO}$ group attacks the $\text{C}=\text{C}$ double bond in the benzene ring forming a cyclic peroxide alkyl radical S3-1-c ($\Delta E_a = 33.6 \text{ kcal mol}^{-1}$). The last is the HO_2 -elimination, where a concerted process of $C_{\alpha}\text{--}\text{O}$ and $C_{\beta}\text{--}\text{H}$ bonds scission forms a closed-shell species S3-1-b and a HO_2 radical byproduct ($\Delta E_a = 33.3 \text{ kcal mol}^{-1}$). The aforementioned results show that the cyclization and HO_2 -elimination reactions are less importance due to their higher barriers.

As depicted in Fig. S1 in the Supplement, the formations of the first generation peroxy radicals S2-2-x from the association reaction $\text{S1-2} + \text{O}_2$ are strongly endothermic ($\Delta E_r = 8.1\text{--}10.4 \text{ kcal mol}^{-1}$), suggesting that they have a significant potential to redissociate back to reactants S1-2 and O_2 . The resulting S2-2-x can undergo through various intramolecular

H-shifts to yield distinct C-centered and O-centered radicals. Among these competing H-shift pathways, hydrogen transfer from the $-\text{OH}$ group to the terminal oxygen of $-\text{OO}$ group has the lowest barrier ($\Delta E_a = 17.4 \text{ kcal mol}^{-1}$). A similar conclusion is also obtained from the association reactions $\text{S1-3} + \text{O}_2$ ($\Delta E_r = 6.6\text{--}7.1 \text{ kcal mol}^{-1}$) and $\text{S1-4} + \text{O}_2$ ($\Delta E_r = 8.1\text{--}11.1 \text{ kcal mol}^{-1}$) that the formations of the first generation peroxy radicals S2-3-x and S2-4-x are thermodynamically unfavorable, and their subsequent intramolecular H-shift barriers are considerably high (Figs. S2 and S3 in the Supplement). Therefore, in the present study, we mainly focus on the subsequent reaction mechanisms of S2-1-x under both low and high NO_x conditions.

In the low- NO_x conditions, the bimolecular reaction with HO_2 radicals is expected to be the dominant sink for RO_2 radicals (Orlando and Tyndall, 2012; Vereecken et al., 2015). Previous studies have reported that the rate coefficient $k_{\text{RO}_2+\text{HO}_2}$ for the reactions of alkyl peroxy radicals with HO_2 radicals is $1.7 \times 10^{-11} \text{ cm}^3 \text{ molec.}^{-1} \text{ s}^{-1}$ (Atkinson and Arey, 2003; Boyd et al., 2003). The typical atmospheric concentration of HO_2 radicals is 20–40 pptv (Wang et al., 2017; Bianchi et al., 2019), resulting in the pseudo-first-order rate constant $k'_{\text{RO}_2+\text{HO}_2} = k_{\text{RO}_2+\text{HO}_2} [\text{HO}_2]$ of 0.01–0.02 s^{-1} . The isomerization reaction of RO_2 radicals is competitive with the bimolecular reactions with HO_2 radicals only when the rate coefficient of intramolecular H-shifts exceeds 0.01–0.02 s^{-1} . In the high- NO_x conditions, the bimolecular reaction of RO_2 radicals with NO is considered to be a dominant sink (Orlando and Tyndall, 2012; Vereecken et al., 2015). The rate coefficient $k_{\text{RO}_2+\text{NO}}$ for the reaction of alkyl peroxy radicals with NO is determined to be $9.0 \times 10^{-12} \text{ cm}^3 \text{ molec.}^{-1} \text{ s}^{-1}$ (Atkinson and Arey, 2003; Bianchi et al., 2019). The typical atmospheric concentration of NO is 0.4–40 ppbv (Wang et al., 2017; Bianchi et al., 2019), leading to the pseudo-first-order rate constant $k'_{\text{RO}_2+\text{NO}} = k_{\text{RO}_2+\text{NO}} [\text{NO}]$ of 0.1–10 s^{-1} . The intramolecular H-shift reaction of RO_2 radicals can compete with the bimolecular reaction with NO only when the rate coefficient of the former case exceeds 10 s^{-1} . Therefore, we use the $k'_{\text{RO}_2+\text{HO}_2}$ (0.01–0.02 s^{-1}) and $k'_{\text{RO}_2+\text{NO}}$ (0.1–10 s^{-1}) values as thresholds to evaluate the relative importance of the isomerization reactions of RO_2 radicals under both low- and high- NO_x conditions. Previous studies have also employed the same methodology to evaluate the relative importance of isomerization and bimolecular reactions of RO_2 radicals during the OH-initiated oxidation of organophosphate esters and alkylbenzenes (Wang et al., 2017; Fu et al., 2024). For the intramolecular H-shift reactions of S2-1-x, the rate coefficient $k_{\text{MC-TST}}$ is estimated to be $1.6 \times 10^{-4} \text{ s}^{-1}$, which is 2–4 orders of magnitude lower than $k'_{\text{RO}_2+\text{HO}_2}$ and $k'_{\text{RO}_2+\text{NO}}$, indicating that the isomerization reaction of S2-1-x is less competitive than the bimolecular reactions with HO_2 radicals and NO .

In the presence of NO , the bimolecular reactions of S2-1-x with NO initially proceed via oxygen-to-oxygen coupling to

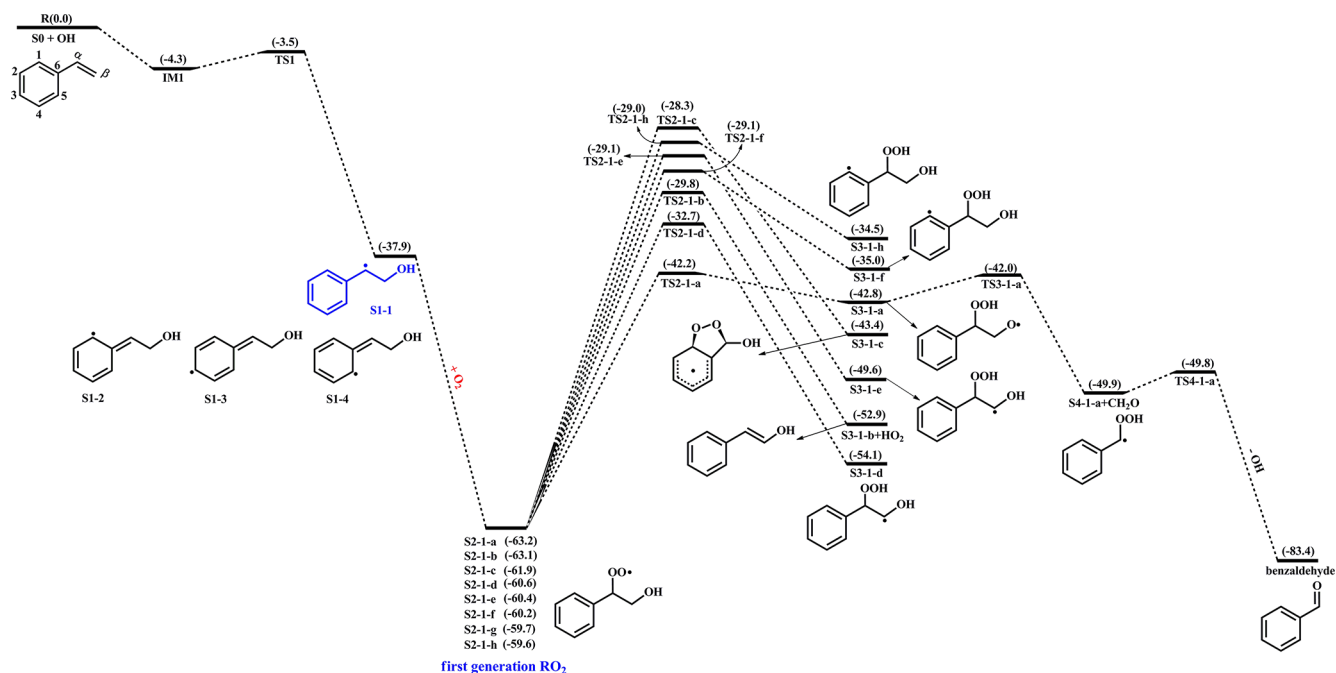


Figure 1. PES for the first-stage oxidation of styrene initiated by OH radicals and the isomerization reactions of S2-1-x at the M06-2X/6-311++G(3df,3pd)//M06-2X/6-31+g(d,p) level.

yield organic nitrites ROONO, which subsequently decompose into benzaldehyde and CH₂OH radical or isomerize to organic nitrates RONO₂. The energy barrier of the rate-limiting step predicted in Wang's study for the formation of benzaldehyde is 28.4 kcal mol⁻¹, which is approximately 4.0 kcal mol⁻¹ greater than that for the formation of RONO₂ (Wang et al., 2015). In the absence of NO, the hydroperoxides ROOH formed from the bimolecular reaction of S2-1-x with HO₂ radicals are anticipated to be the dominant products. The aforementioned results are further confirmed by the recent smog chamber experiment study that C₇ and C₈ series products, as well as organic nitrates are the main components of SOA in the OH-initiated oxidation of styrene under different NO_x conditions (Yu et al., 2022b). Considering that the extensive studies on the OH-initiated oxidation of benzaldehyde have done (Sebbar et al., 2011; Zhao et al., 2022; Iuga et al., 2008), this study primarily focuses on the multi-generation •OH oxidation mechanisms of ROOH and RONO₂ under both low- and high-NO_x conditions.

3.2 Second generation •OH oxidation mechanisms of 1st-ROOH and 1st-RONO₂

The first generation products, including hydroperoxides 1st-ROOH and organic nitrates 1st-RONO₂, include multiple conformers. To obtain the global minimum of 1st-ROOH and 1st-RONO₂, the conformer search is performed by using the Molclus program. The resulting structures are initially optimized at the M06-2X/6-31+g(d,p) level, then the single point

energies are calculated at the M06-2X/6-311++G(3df,3pd) level. The global minimum structures of 1st-ROOH (S4) and 1st-RONO₂ (S5) are presented in Fig. S4 in the Supplement.

3.2.1 The oxidation mechanism of 1st-ROOH initiated by OH radicals

The reaction 1st-ROOH (S4) + •OH proceeds through the addition of OH radicals to either side of the benzene ring to yield various alkyl radicals, as depicted in Fig. 2. In the present study, *syn*-OH-addition is defined as the scenario in which the addition of OH radicals occurs at the same side as the -OOH group, while *anti*-OH-addition is referred to the scenario in which the addition of OH radicals occurs at the opposite side as the -OOH group. For the *syn*-OH-addition reactions, the addition of OH radicals to the C1-site of 1st-ROOH (S4) exhibits the lowest barrier ($\Delta E_a = 3.6$ kcal mol⁻¹) due to the stability of the formed product, P_{S4-add1'}. A similar conclusion is also obtained from the *anti*-OH-addition reactions that the OH-addition pathway occurring at the C1-site is favorable ($\Delta E_a = 0.8$ kcal mol⁻¹). Notably, the preferred OH-addition pathway in the *anti*-OH-addition reactions exhibits greater competitiveness compared to that in the *syn*-OH-addition reactions. It can be explained by the greater steric hindrance present in the latter reaction. In order to further evaluate the reliability of our results, ΔE_a of all the *syn*-OH-addition and *anti*-OH-addition reactions are recalculated using the DLPNO-CCSD(T)/aug-cc-pVTZ//M06-2X/6-311+G(d,p) method. As shown in Ta-

ble S3 in the Supplement, the ΔE_a values obtained using the M06-2X/6-311++G(3df,3pd) method are in good agreement with those derived from the DLPNO-CCSD(T)/aug-cc-pVTZ method. The largest deviation and the average absolute deviation are 1.2 and 0.9 kcal mol⁻¹, respectively, indicating that the M06-2X/6-311++G(3df,3pd) method employed in this study is reliable. Based on the values of ΔE_a obtained using the DLPNO-CCSD(T)/aug-cc-pVTZ method, it can also be concluded that the addition of OH radicals to C1-site, occurring at the opposite direction relative to the -OOH group, is energetically favorable. The rate coefficients of the addition of OH radicals to the different sites of 1st-ROOH are calculated to be 8.2×10^{-12} (C1-site), 5.8×10^{-15} (C2-site), 8.3×10^{-15} (C3-site), 8.6×10^{-15} (C4-site), 2.7×10^{-12} (C5-site) and 4.1×10^{-13} (C6-site) cm³ molec.⁻¹ s⁻¹, respectively. The branching ratios for •OH addition to the C1, C5 and C6 sites are predicted to be 72.4 %, 23.8 % and 3.6 %, respectively, while the sum of branching ratios for •OH addition to other carbon sites is less than 1 %.

Our result is opposite to Zhang's finding that the addition of OH radicals to C6-site would be the most favorable pathway (Zhang et al., 2024). The discrepancy can be explained by the following three factors: (1) The 1st-ROOH conformer selected in the Zhang's study is not the global minimum. In the present study, the global minimum conformer of 1st-ROOH, identified through the conformer search, is found to be 2.2 kcal mol⁻¹ lower than the 1st-ROOH structure selected in the Zhang's study. (2) The pre-reactive complexes are not considered in the Zhang's study. The addition of OH radicals to C1-, C2-, C3- and C6-sites, occurring at the opposite direction relative to the -OOH group, are merely considered in the Zhang's study. They found that the apparent energy barrier of the addition of OH radicals to C6-site is smallest, and is therefore expected to be the favorable pathway. Actually, these OH-addition reactions are modulated by the pre-reactive complexes. It may be inappropriate to determine the favorable pathway based solely on apparent activation energy without considering the pre-reaction complexes. (3) From a geometric perspective, the addition of OH radicals to C6-site is associated with greater steric hindrance compared to other sites, as C6-atom connects with a larger functional group. Based on the aforementioned discussions, we believe that the addition of OH radicals to C6-site is unlikely to be the dominant pathway. Our calculations also confirm that the addition of OH radicals to C6-site is less important compared to that at the C1-site.

Our conclusion is further supported by the reaction toluene + •OH that the *ortho*-OH-addition reaction exhibits significant dominance, with the branching ratio of up to 69.8 %–75.8 % (Ji et al., 2017; Zhang, 2019; Wu et al., 2020). Considering the high reactivity of *ortho*-OH-addition in the reactions toluene + •OH and 1st-ROOH (S4) + •OH, the substitute effects of the -CH₃ and -OOH groups are explicitly discussed in the present study. Notably, the -CH₃ group in

toluene is bonded to the C6 atom, and the -OOH group in 1st-ROOH is bonded to the C α atom, as depicted in Fig. S5 in the Supplement. The optimized geometries of toluene and 1st-ROOH and the NPA atomic charges of all the carbon atoms in the benzene ring are displayed in Fig. S5. The C–C bond lengths and the C–C–C bond angles in the benzene ring of toluene are approximately 1.39 Å and 120°, respectively, which are consistent with those in the benzene ring of 1st-ROOH. The aforementioned results show the effect of the -CH₃ and -OOH groups on the geometric structure of benzene ring is negligible. From the perspective of NPA atomic charges, the charges on the C1 (-0.246 e) and C5 (-0.246 e) atoms are more greater than those on the other carbon atoms in the benzene ring of toluene. And the OH-adduct formed from the *ortho*-OH-addition reaction exhibits the greater stability. These results indicate that the -CH₃ group is a typical *ortho*-directing substituent and exerts an activating effect on the *ortho*-site of the benzene ring, which explains why the *ortho*-OH-addition reaction is predominant in the reaction toluene + •OH. Compared with the charges on the carbon atoms in the benzene ring of toluene, the charges on C1 and C6 atoms increase by 0.013 e and 0.057 e, respectively, in 1st-ROOH, which can be attributed to the electron-withdrawing effect of the -OOH group. The charge on the C1 atom (-0.259 e) is the highest, and the stability of the resulting OH-adduct is the greatest, implying that the addition of OH radicals to C1-site is dominant in the reaction 1st-ROOH + •OH. Therefore, a direct comparison of the favorable OH-addition pathway in the reactions toluene + •OH and 1st-ROOH (S4) + •OH is performed in this study.

The formed product P_{S4-add1} includes two conjugate double bonds (C₂=C₃ and C₄=C₅), which can readily isomerize to P_{S4-add2} and P_{S4-add3}, as evident from Fig. S6 in the Supplement. In the presence of O₂, the attack of an O₂ molecule on the C-centered site of P_{S4-add1}, P_{S4-add2}, and P_{S4-add3} proceed via the barrierless processes to produce the second generation peroxy radicals P_{S4-add1-a/s}, P_{S4-add2-a/s} and P_{S4-add3-a/s}. The O₂-addition reaction occurring at the same direction as the -OOH group is defined as *syn*-O₂-addition, while the O₂-addition reaction occurring at the opposite direction as the -OOH group is defined as *anti*-O₂-addition. For the reaction P_{S4-add1} + O₂ → P_{S4-add1-a/s}, ΔE_r of *anti*-O₂-addition is -5.8 kcal mol⁻¹, which is lower than that of *syn*-O₂-addition by 0.4 kcal mol⁻¹, suggesting that *anti*-O₂-addition is preferable over *syn*-O₂-addition in energy. For the reactions P_{S4-add2} + O₂ → P_{S4-add2-a/s} and P_{S4-add3} + O₂ → P_{S4-add3-a/s}, it can be concluded the same by the ΔE_r values that *anti*-O₂-addition reaction is energetically feasible.

The resulting P_{S4-add1-a/s} can proceed intramolecular cyclization reaction, where the attack of end-site oxygen atom of the -OO group on C2-site of the C₂=C₃ double bond, leading to the formation of peroxide bicyclic alkyl radicals. ΔE_a and ΔE_r of the reaction P_{S4-add1-a} → P_{S4-add1-a-1} are 11.8 and -16.8 kcal mol⁻¹, respectively, which are lower

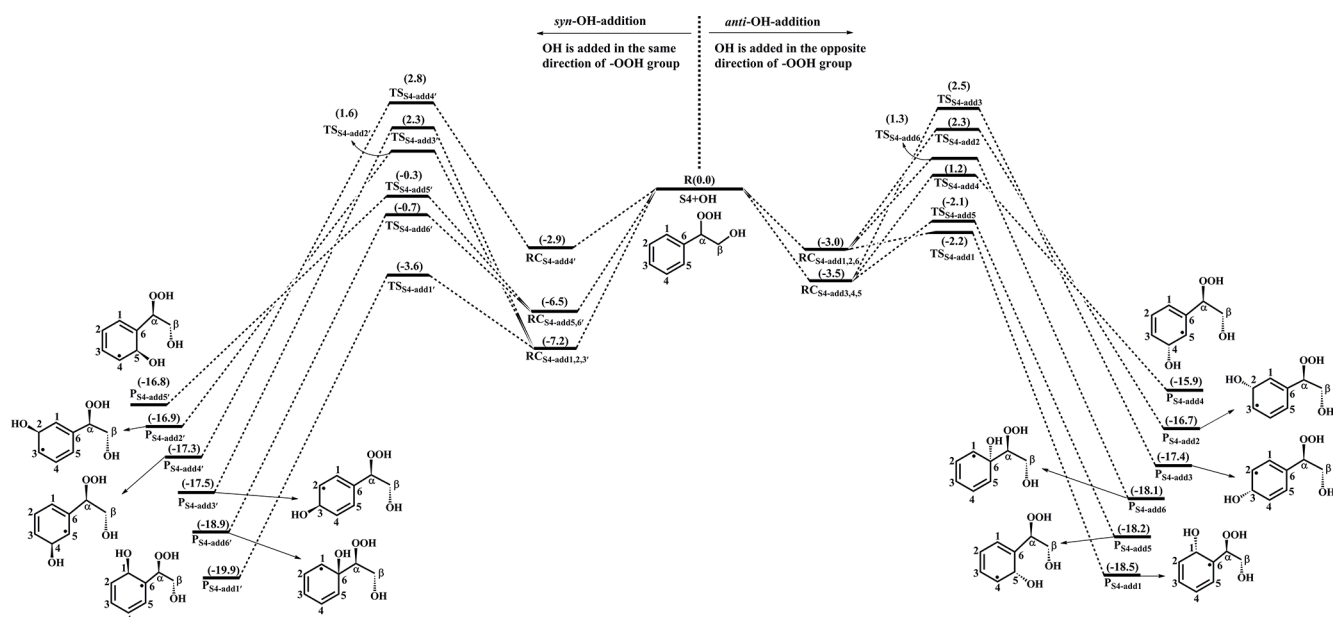


Figure 2. PES for the oxidation of 1st-ROOH(S4) initiated by OH radicals at the M06-2X/6-311++G(3df,3pd)/M06-2X/6-31+g(d,p) level.

than those of the reaction $\text{P}_{\text{S4-add1-s}} \rightarrow \text{P}_{\text{S4-add1-s-1}}$ by 3.9 and 2.2 kcal mol⁻¹, respectively. The aforementioned results reveal that the intramolecular cyclization reaction of *anti*-O₂-addition product $\text{P}_{\text{S4-add1-a}}$ is favorable on both thermochemically and kinetically. A similar conclusion is also derived from the intramolecular cyclization reactions of *anti*-O₂-addition products $\text{P}_{\text{S4-add2-a}}$ and $\text{P}_{\text{S4-add3-a}}$. Notably, the barriers of the intramolecular cyclization reactions $\text{P}_{\text{S4-add2-a}} \rightarrow \text{P}_{\text{S4-add2-a-1}}$ ($\Delta E_a = 31.1$ kcal mol⁻¹) and $\text{P}_{\text{S4-add2-a}} \rightarrow \text{P}_{\text{S4-add2-a-2}}$ ($\Delta E_a = 34.6$ kcal mol⁻¹) are extremely high, making them insignificant in the atmosphere. The tautomerization between $\text{P}_{\text{S4-add1-a-1}}$ and $\text{P}_{\text{S4-add3-a-1}}$ readily occurs due to the existence of resonance structures, and it is therefore that the latter conformer is selected as a prototype for the investigating of its subsequent reaction mechanism.

The formed $\text{P}_{\text{S4-add3-a-1}}$ can combine with an O₂ molecule leading to the third generation peroxy radicals (also called as peroxide bicyclic peroxy radicals, BPR) $\text{P}_{\text{S4-add3-a-2}}$, and the lowest energy conformer is presented in Fig. S7 in the Supplement. The isomerization of $\text{P}_{\text{S4-add3-a-2}}$ may undergo through a concerted process of the cleavage of –O–O– bridge bond and C₁–C₂ bond as well as hydrogen atom transfer from the hydroxyl group to the bridge oxygen atom, yielding a new peroxy radical ($\Delta E_a = 28.5$ kcal mol⁻¹). The room temperature rate coefficient is calculated to be 3.0×10^{-9} s⁻¹, which is several orders of magnitude low than the typical pseudo-first-order rate constants $k'_{\text{RO}_2+\text{HO}_2}$ (0.01–0.02 s⁻¹) and $k'_{\text{RO}_2+\text{NO}}$ (0.1–10 s⁻¹), suggesting that the isomerization reaction is less importance in the atmosphere. Therefore, the bimolecular reactions of $\text{P}_{\text{S4-add3-a-2}}$ with

HO₂ radicals with NO are mainly taken into consideration in this study.

In the pristine environments, $\text{P}_{\text{S4-add3-a-2}}$ can react with HO₂ radicals resulting in the formation of the second generation products, bicyclic hydroperoxide 2nd-ROOH (S6) and peroxide bicyclic alkoxy radical (BAR) $\text{P}_{\text{S4-add3-a-3}}$, as depicted in Fig. S7. For the subsequent reactions of S6 initiated by OH radicals, the detailed mechanisms are discussed in Sect. 3.3.1. From Fig. 3, it can be seen that the unimolecular decomposition of $\text{P}_{\text{S4-add3-a-3}}$ involves two kinds of pathways. One is the ring-opening reaction, where the breakage of C₅–C₆ bond produces an alkyl radical S7 ($\Delta E_a = 5.9$ kcal mol⁻¹). The other is cyclization reaction, where the attack of oxygen atom of O-centered site on the C₄-site of the C₃=C₄ double bond generates the ring-retaining alkyl radical S15 ($E_a = 8.0$ kcal mol⁻¹). The branching ratios for the formation of S7 and S15 are predicted to be 74.7 % and 25.3 %, respectively.

As shown in Fig. 3, S7 decomposes through the barrierless rupture of –O–O– bridge bond to form alkoxy radical S8-x, which includes five possible conformers as presented in Fig. S8 in the Supplement. The Boltzmann populations of different conformers are listed in Table S4 in the Supplement. S8-x can undergo various intramolecular H-shifts, in which a hydrogen atom is transferred from different carbon atoms to O-centered site, forming the alkyl radicals. Among the competing H-shift reactions, 1,5 H-shift occurring at the –C₅(O)H group exhibits the smallest barrier ($\Delta E_a = 0.6$ kcal mol⁻¹), and $k_{\text{MC-TST}}$ is calculated to be 8.2×10^9 s⁻¹ at ambient temperature (Table S5 in the Supplement). The formed S8-c-P can readily isomerize to S9 due to its resonance stabilized structure. The unimolecular decom-

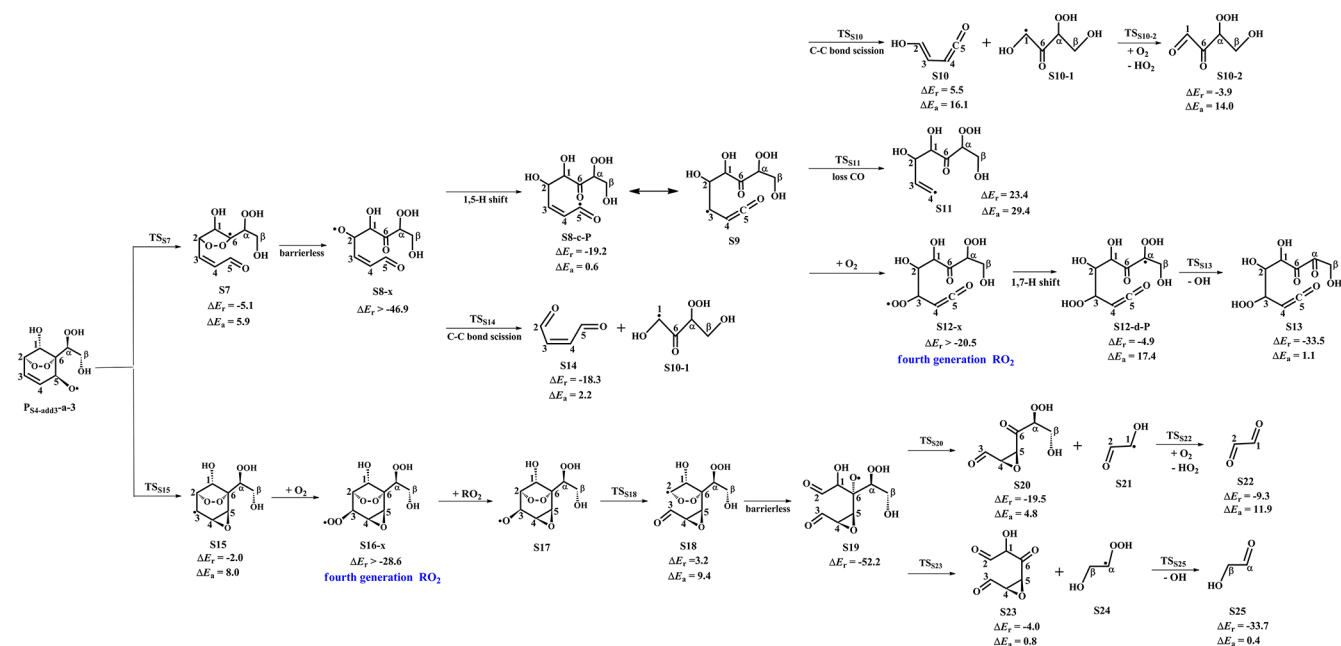


Figure 3. PES for the unimolecular decomposition of $\text{PS}_{4\text{-add}3\text{-a-}3}$ and its subsequent reactions at the M06-2X/6-311++G(3df,3pd)//M06-2X/6-31+g(d,p) level.

position of S9 can proceed through the C₁–C₂ bond scission to produce a ketene-enol S10 and an alkyl radical S10-1 ($\Delta E_a = 16.1 \text{ kcal mol}^{-1}$), followed by reaction with O₂ leading to a HO₂ radical and a 1,2-dicarbonyl compound S10-2 ($\Delta E_a = 14.0 \text{ kcal mol}^{-1}$). Alternatively, S9 may undergo via the elimination of CO to generate an alkyl radicals S11 ($\Delta E_a = 29.4 \text{ kcal mol}^{-1}$). The aforementioned results show that the formation of S10 and S10-1 is energetically favorable, with the rate coefficient k_{S10} of 26.1 s^{-1} .

In the presence of O₂, the attack of an O₂ molecule on the C-centered sites of S9 leads to the fourth generation peroxy radical S12-x ($\Delta E_r > -20.5 \text{ kcal mol}^{-1}$). Adopting the rate coefficient $k_{\text{R}+\text{O}_2}$ of $6.0 \times 10^{-12} \text{ cm}^3 \text{ molec.}^{-1} \text{ s}^{-1}$ for the reactions of alkyl radicals with O₂, and the atmospheric O₂ concentration of $5 \times 10^{18} \text{ molec. cm}^{-3}$ (Ma et al., 2021), the pseudo-first-order rate constant $k'_{\text{R}+\text{O}_2} = k_{\text{R}+\text{O}_2} [\text{O}_2]$ is $3.0 \times 10^7 \text{ s}^{-1}$. The unimolecular decomposition of alkyl radicals is competitive only when their decay rate exceeds $3.0 \times 10^7 \text{ s}^{-1}$. $k'_{\text{R}+\text{O}_2}$ is about six orders of magnitude greater than k_{S10} , indicating that the unimolecular decomposition of S9 is less importance. As shown in Fig. S9 in the Supplement, S12-x can proceed various intramolecular H-shift reactions, where hydrogen atom migrates from the different carbon sites or hydroxyl groups to the terminal oxygen atom of the –OO group, resulting in the formation of QOOH radicals and alkoxy radicals. Among these competing H-shift reactions, the 1,7-H transfer at the C α -site leading to the formation of S12-d-P exhibits the smallest barrier ($\Delta E_a = 17.4 \text{ kcal mol}^{-1}$). Then, it decomposes to yield an OH radical and a closed-shell product S13 containing

a hydroperoxide, three hydroxyl and three carbonyl groups ($\Delta E_a = 1.1 \text{ kcal mol}^{-1}$).

S8-x can proceed through the C₁–C₂ bond scission to yield an unsaturated 1,4-dicarbonyl species S14 and an alkyl radical S10-1 ($\Delta E_a = 2.2 \text{ kcal mol}^{-1}$), with the rate coefficient of $2.1 \times 10^{10} \text{ s}^{-1}$. Notably, both the 1,5 aldehyde H-shift and C₁–C₂ bond scission reactions yield a closed-shell species S10-2 with up to five oxygen atoms, and the branching ratios are predicted to be 28.1 % and 71.9 %, respectively. The result is further supported by the previous study that the proportion of aldehyde H-shift products constitutes about one third of the total products in the reaction benzene + •OH (Wang et al., 2020b).

As shown in Fig. 3, S15 can further react with O₂ leading to the fourth generation peroxy radical S16-x, which can proceed either intramolecular H-shifts forming QOOH radicals (Fig. S10 in the Supplement), or reactions with RO₂ radicals and NO forming alkoxy radical S17. Notably, the barriers of intramolecular H-shifts are extremely high ($\Delta E_a > 34.6 \text{ kcal mol}^{-1}$), making them less importance in the atmosphere. The transformation of S17 undergoes through the breakage of C₂–C₃ bond to produce an alkyl radical S18 ($\Delta E_a = 9.4 \text{ kcal mol}^{-1}$), followed by fragmentation into an alkoxy radical S19 via the barrierless rupture of the –O–O– bridge bond. Then, S19 dissociates to an OH radical, a glycolaldehyde S25 and a C₆-epoxide product S23 bearing a hydroxy and three carbonyl groups, being the dominant pathway. The regeneration of OH radicals drives the successive autoxidation of styrene, eventually leading to the production of multifunctional products.

3.2.2 The oxidation mechanism of 1st-RONO₂ initiated by OH radicals

The OH-initiated oxidation of 1st-RONO₂ (S5) proceeds through the addition of OH radicals to different carbon sites in the benzene ring to form various alkyl radicals P_{S5-addx}, as depicted in Fig. 4. Among the competing OH-addition reactions, the OH-addition reaction at the C1-site, which proceeds on the opposite direction as the –ONO₂ group, has the smallest barrier (R_{S5-add1}, $\Delta E_a = 0.4 \text{ kcal mol}^{-1}$) due to the stability of the formed product P_{S5-add1}. The result again shows that the *ortho*-addition reaction is energetically feasible. P_{S5-add1} may isomerize to two other resonance structures, namely, P_{S5-add2} and P_{S5-add3}. For the reaction P_{S5-add1} + O₂, O₂ may add on either the opposite (*anti*-O₂-addition) or the same direction (*syn*-O₂-addition) relative to the –NO₃ group, leading to the second generation peroxy radicals P_{S5-add1-a} and P_{S5-add1-s} (Fig. S11 in the Supplement). The exoergicity of these two reactions are –6.7 and –4.4 kcal mol^{–1}, respectively, suggesting that the *anti*-O₂-addition reaction is thermochemically favorable. Next, they can isomerize via a cyclization process to yield P_{S5-add1-a-1} and P_{S5-add1-s-1} with the ΔE_a of 13.3 and 18.1 kcal mol^{–1}. This result shows that the cyclization reaction of *anti*-O₂-addition product P_{S5-add1-a} is kinetically feasible. A similar conclusion is also obtained from the reaction P_{S5-add3} + O₂ that the formation of *anti*-O₂-addition product P_{S5-add3-a-1} is dominant. Due to the existence of the conjugate double bond, it facilitates the tautomerization between P_{S5-add1-a-1} and P_{S5-add3-a-1}. Therefore, we mainly focus on the subsequent chemistry of P_{S5-add3-a-1} in the present study.

P_{S5-add3-a-1} can further react with an O₂ molecule leading to the third generation peroxy radicals P_{S5-add3-a-2}, which include multiple conformers. The lowest energy conformer resulting from conformer search is presented in Fig. S12 in the Supplement. In urban environments, the bimolecular reaction of P_{S5-add3-a-2} with NO yields the second generation products, a bicyclic organic nitrate 2nd-RONO₂ (S26) and a BAR P_{S5-add3-a-3}, as displayed in Fig. S12. The detailed mechanism of OH-initiated oxidation of S26 is discussed in Sect. 3.3.2. As shown in Fig. 5, P_{S5-add3-a-3} can either proceed via a ring opening process to form an alkyl radical S27 ($\Delta E_a = 7.3 \text{ kcal mol}^{-1}$), or undergo through a cyclization process to generate an epoxide species S35 ($\Delta E_a = 8.5 \text{ kcal mol}^{-1}$). The branching ratios of these two reactions are predicted to be 69.2 % and 30.8 %, respectively. Notably, the branching ratio of cyclization reaction of P_{S5-add3-a-3} increases by 5.5 % compared to that of cyclization reaction of P_{S4-add3-a-3}, suggesting that the –ONO₂ substitution is beneficial to cyclization reaction.

The degradation of S27 proceeds through the barrierless scission of –O–O– bridge bond to form S28-x, and the Boltzmann populations of different conformers are listed in Table S6 in the Supplement. S28-x can undergo via various intramolecular H-shifts to produce QOOH radicals, in

which hydrogen atom transfer from the –C(O)H group to the terminal oxygen atom of the –OO group forming S28-e-P has the smallest barrier ($\Delta E_a = 2.0 \text{ kcal mol}^{-1}$) (Fig. S13 in the Supplement). S28-e-P can readily isomerize to S29, which includes two distinct decomposition pathways. One is the C₁–C₂ bond cleavage, yielding a ketene-enol S30 and an alkyl radical S30-1 ($\Delta E_a = 17.8 \text{ kcal mol}^{-1}$), followed by reaction with O₂ to form a HO₂ radical and a 1,2-dicarbonyl species S30-2 ($\Delta E_a = 11.7 \text{ kcal mol}^{-1}$). The other is the elimination of CO to generate an alkyl radical S31 ($\Delta E_a = 24.8 \text{ kcal mol}^{-1}$), but the barrier is considerably high, making this pathway less competitive. The rate coefficient for the formation of S30 and S30-1 is calculated to be 14.4 s^{-1} , which is about six orders of magnitude lower than the pseudo-first-order rate constant k'_{R+O_2} , indicating that the unimolecular decomposition of S29 is insignificant.

In the presence of O₂, the bimolecular reaction of S29 with O₂ produces the fourth generation peroxy radicals S32-x, comprising five energetically similar conformers as shown in Fig. S14 in the Supplement. For the 1,7-H transfer reaction, hydrogen atom at the C α -site can be transferred through an eight-membered ring transition state to generate an alkyl radical S32-d-P ($\Delta E_a = 23.3 \text{ kcal mol}^{-1}$), followed by the elimination of NO₂ forming a closed product S33 ($\Delta E_a = 1.0 \text{ kcal mol}^{-1}$). S33 and S13 are isomeric species, with the former exhibiting more stability than the latter. S28-x can proceed through the cleavage of C₁–C₂ bond to generate an unsaturated 1,4-dicarbonyl compound S34 and an alkyl radical S30-1. The rare coefficients of the 1,5 aldehyde H-shift and C₁–C₂ bond scission reactions are predicted to be 1.7×10^9 and $5.8 \times 10^9 \text{ s}^{-1}$ (Table S7 in the Supplement), respectively, with the branching ratios of 23 % and 77 %. S30-1, formed from the above mentioned two pathways, may undergo through H-abstraction by O₂ to yield an organic nitrate S30-2 bearing a hydroxyl and two carbonyl groups ($\Delta E_a = 11.7 \text{ kcal mol}^{-1}$).

S35 can combine with an O₂ molecule forming the fourth generation peroxy radicals S36-x, which have five possible conformers as shown in Fig. S15 in the Supplement. S36-x can proceed either intramolecular H-shifts forming QOOH radicals, or reaction with RO₂ radicals and NO generating alkoxy radical S37. However, the barriers of intramolecular H-shifts are extremely high ($\Delta E_a > 31.3 \text{ kcal mol}^{-1}$), making them less importance in the atmosphere. The degradation of S37 initially proceeds via the breakage of C₂–C₃ bond to form S38 ($\Delta E_a = 9.2 \text{ kcal mol}^{-1}$), followed by decomposition into an alkoxy radical S39 via the barrierless scission of –O–O– bridge bond. The dominant pathway of the unimolecular decomposition of S39 is the formation of a glyoxal and a C₆-epoxide species S40-1 bearing a –NO₃, a hydroxyl and two carbonyl groups. This process differs from the unimolecular decay of S19, where the favorable pathways is the formation of a tricarbonyl compound S23. The aforementioned results reveal that the preferable pathway is strongly dependent on the breakage of C–C bond associated with the

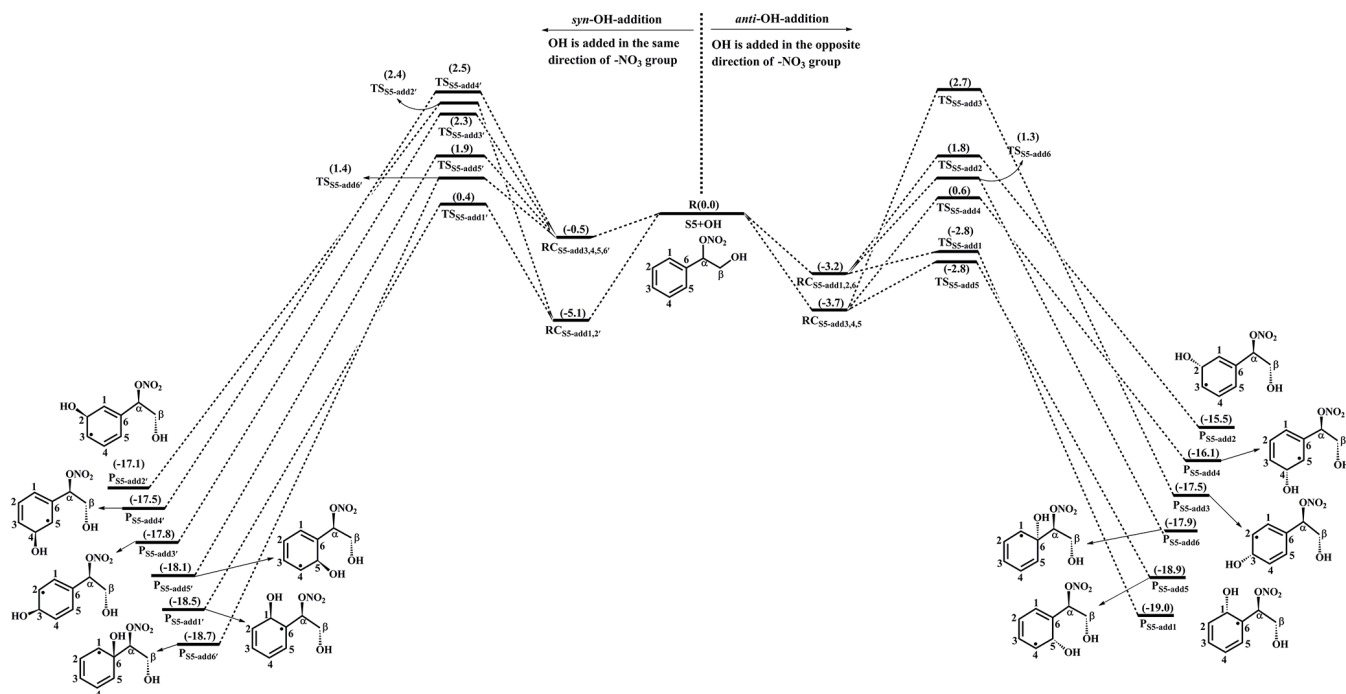


Figure 4. PES for the oxidation of 1st-RONO₂(S5) initiated by OH radicals at the M06-2X/6-311++G(3df,3pd)/M06-2X/6-31+g(d,p) level.

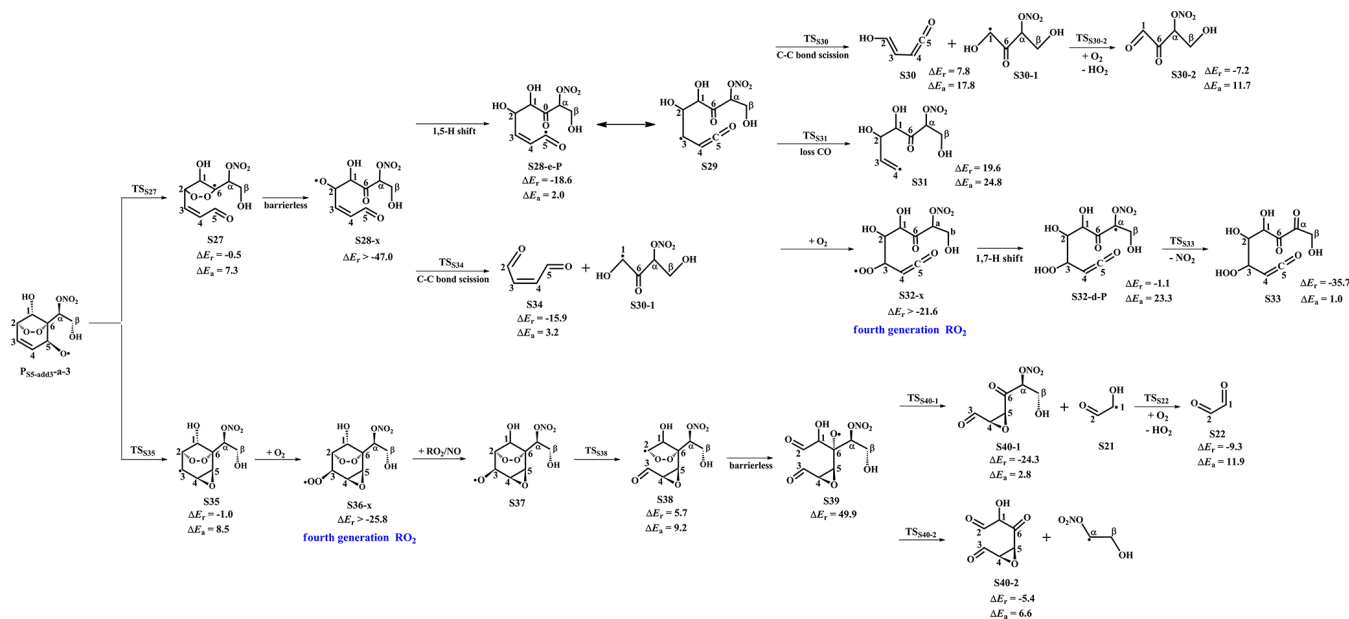


Figure 5. PES for the unimolecular decomposition of P_{S5-add3}-a-3 and subsequent reactions at the M06-2X/6-311++G(3df,3pd)/M06-2X/6-31+g(d,p) level.

property of substituents in the decomposition of alkoxy radicals.

3.3 Third generation $\cdot\text{OH}$ oxidation mechanisms of 2nd-ROOH and 2nd-RONO₂

The second generation products, bicyclic hydroperoxide 2nd-ROOH and bicyclic organic nitrate 2nd-RONO₂, have multiple possible conformers. The global minimum structures of 2nd-ROOH (S6) and 2nd-RONO₂ (S26) resulting from the conformer search are presented in Figs. S7 and S12, respectively.

3.3.1 The oxidation mechanism of 2nd-ROOH initiated by OH radicals

OH-initiated oxidation of 2nd-ROOH (S6) can either undergo through the addition of OH radicals to either side of the C₃=C₄ double bond to generate the alkyl radicals, or proceed via H-abstraction from the different carbon sites to produce the alkyl radicals and alkoxy radicals, as shown in Figs. S16 and S17 in the Supplement. For the OH-addition reactions, *syn*-OH-addition is defined as the addition of OH radicals on the same side as the –OOH group, while *anti*-OH-addition is referred to the addition of OH radicals on the opposite side as the –OOH group. The addition of OH radicals to the C3-site of the C₃=C₄ double bond forming the product P_{S6-abs3} has the smallest barrier ($\Delta E_a = 2.4 \text{ kcal mol}^{-1}$) and the exoergicity of $-33.5 \text{ kcal mol}^{-1}$. For the H-abstraction reactions, the abstraction of hydrogen atom at the C5-site is the most favorable pathway ($\Delta E_a = 3.6 \text{ kcal mol}^{-1}$) and the exoergicity of $-20.2 \text{ kcal mol}^{-1}$. It is mainly because that the presence of an allyl group enhances the stability of the resulting product P_{S6-abs5}. Notably, the abstraction of hydrogen atom at the C2-site proceeds through a concerted process of C₂–H bond and –O–O– bridge bond rupture, leading to the formation of an alkoxy radical P_{S6-abs2} ($\Delta E_a = 7.2 \text{ kcal mol}^{-1}$). This reaction is expected to be less importance due to its higher energy barrier. The rate coefficient of the favorable OH-addition reaction is calculated to be $6.4 \times 10^{-11} \text{ cm}^3 \text{ molec.}^{-1} \text{ s}^{-1}$, which is about one order of magnitude greater than that of the preferable H-abstraction reaction ($4.1 \times 10^{-12} \text{ cm}^3 \text{ molec.}^{-1} \text{ s}^{-1}$). Based on the above discussion, it can be concluded that OH-addition reaction is favorable on both thermochemically and kinetically. This conclusion is further supported by the $\cdot\text{OH} + \text{alkene}$ reaction systems that OH-addition pathways are predominant (Chen et al., 2021; Yang et al., 2017; Arathala and Musah, 2024).

As depicted in Fig. S18 in the Supplement, the unimolecular decay of the product P_{S6-add3} resulting from the favorable OH-addition reaction proceeds through a cyclization process to yield an epoxide compound S41 and an OH radical byproduct with the ΔE_a of $15.3 \text{ kcal mol}^{-1}$ and the rate coefficient k_{R41} of $1.8 \times 10^2 \text{ s}^{-1}$, or undergoes via intramolecular 1,4 H-shift to form a peroxy radical S42 with the ΔE_a

of $21.8 \text{ kcal mol}^{-1}$ and the rate coefficient k_{R43} of 1.9 s^{-1} , or proceeds via the elimination of hydrogen atom to produce an alkene S43 with the ΔE_a of $37.9 \text{ kcal mol}^{-1}$. Based on the values of ΔE_a and the corresponding rate coefficients, the dominant pathway of the unimolecular decomposition of P_{S6-add3} is the formation of S41. In the presence of O₂, the pseudo-first-order rate constant k'_{R+O_2} of the reactions of alkyl radicals with O₂ is $3.0 \times 10^7 \text{ s}^{-1}$, which is about five orders of magnitude greater than k_{R41} , suggesting that the unimolecular decomposition of P_{S6-add3} is insignificant.

As shown in Fig. 6, the fourth generation peroxy radicals S44-x formed in the addition reaction P_{S6-add3} + O₂ can either proceed via intramolecular H-shits to form QOOH, or undergo through self- or cross-reactions to yield an alkoxy radical S45. Due to the considerably high barriers of intramolecular H-shifts, they are deemed to be negligible under atmospheric conditions. S45 can convert into an alkyl radical S46 through the cleavage of C₄–C₅ bond, or dissociate to an alkyl radical S50 via the rupture of C₃–C₄ bond. The barrier of the former reaction is $3.9 \text{ kcal mol}^{-1}$, which is lower than that of the latter pathway by $2.6 \text{ kcal mol}^{-1}$, indicating that the formation of S46 is kinetically preferable. Then, S46 decomposes into an OH radical byproduct and a C₈-product S47 bearing a –OOH, a peroxide bridge, two carbonyls, and three hydroxy groups, which is expected to be the dominant pathway owing to its lower barrier. The rate coefficient k_{RS47} is estimated to be $1.8 \times 10^9 \text{ s}^{-1}$, which is about two orders of magnitude greater than the pseudo-first-order rate constant k'_{R+O_2} ($3.0 \times 10^7 \text{ s}^{-1}$). The result reveals that the unimolecular decomposition of S46 is more competitive than the bimolecular reaction with O₂. The formed OH radicals can once again participate in the oxidations of styrene and its multifunctional products, continuing these processes until they are completely consumed.

3.3.2 The oxidation mechanism of 2nd-RONO₂ initiated by OH radicals

OH-initiated oxidation of 2nd-RONO₂ (S26) includes four different OH-addition pathways and five different H-abstraction pathways, as displayed in Figs. S19 and S20 in the Supplement. For the OH-addition reactions, the attack of OH radicals on the C3-site of the C₃=C₄ double bond forming the product P_{S26-add3}, occurring on the same direction relative to the –ONO₂ group, is found to be the favorable pathway ($\Delta E_a = 2.4 \text{ kcal mol}^{-1}$, $\Delta E_r = -33.6 \text{ kcal mol}^{-1}$). For the H-abstraction reactions, the abstraction of hydrogen atom at the C5-site is identified as the preferable pathway ($\Delta E_a = 5.7 \text{ kcal mol}^{-1}$, $\Delta E_r = -20.1 \text{ kcal mol}^{-1}$) due to the enhanced stability of the resulting product P_{S26-add5} by the presence of an allyl group. By comparing the values of ΔE_a and ΔE_r of the favorable OH-addition and H-abstraction pathways, it can be concluded that the former case is dominant on both thermochemically and kinetically. This conclusion is consistent with the result from the reaction

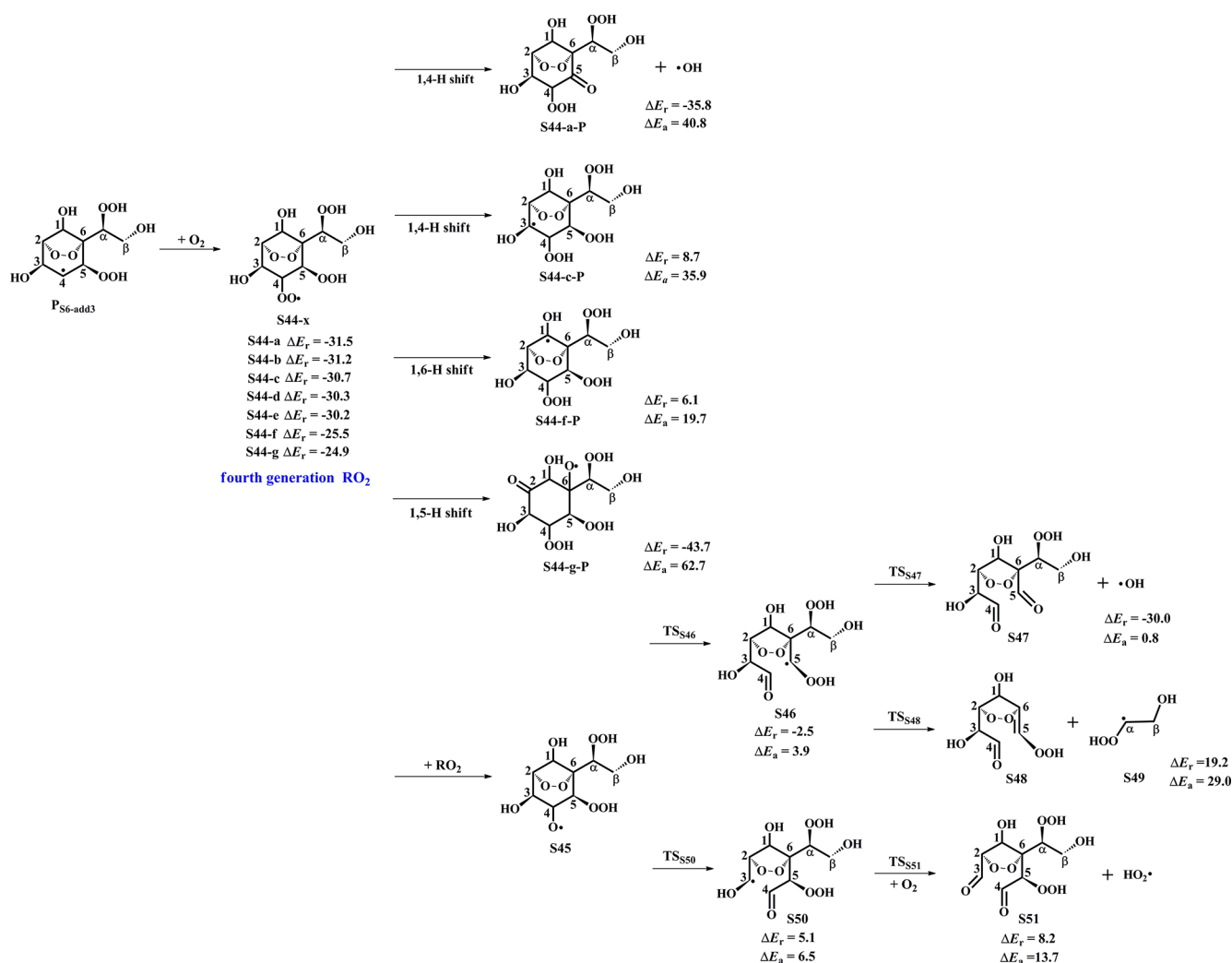


Figure 6. PES for the subsequent reactions of $P_{S6-add3}$ in the presence of O_2 at the M06-2X/6-311++G(3df,3pd)/M06-2X/6-31+g(d,p) level.

2nd-ROOH (S6) + $\cdot OH$ that OH-addition is more competitive than H-abstraction.

The product $P_{S26-add3}$ arising from the favorable OH-addition pathway has three potential unimolecular decay pathways, as depicted in Fig. S21 in the Supplement: (1) $P_{S26-add3}$ dissociates to an epoxide S52 and a NO_2 molecule through a cyclization process with the ΔE_a of $18.5\text{ kcal mol}^{-1}$ and the rate coefficient k_{R52} of 0.4 s^{-1} ; (2) $P_{S26-add3}$ isomerizes to an alkyl radical S53 via the intramolecular 1,2 H-shift ($\Delta E_a = 40.0\text{ kcal mol}^{-1}$); (3) $P_{S26-add3}$ converts into an alkene S54 via the elimination of hydrogen atom ($\Delta E_a = 39.1\text{ kcal mol}^{-1}$). Based on the value of ΔE_a and the corresponding rate coefficient, the dominant pathway of the unimolecular decomposition of $P_{S26-add3}$ is the formation of S52. k_{R52} is about seven orders of magnitude lower than the pseudo-first-order rate constant k'_{R+O_2} , indicating that the unimolecular decomposition of $P_{S26-add3}$ is less importance.

In the presence of O_2 , $P_{S26-add3}$ can react with an O_2 molecule leading to the formation of the fourth generation peroxy radicals S55-x, comprising seven possible conformers as shown in Fig. 7. For the intramolecular H-shifts of S55-x, not all of reactants (S55-c, S55-d and S55-e) have the suitable conformers that allow for the pathways across the reaction barriers. The barriers of intramolecular H-shifts are considerably high ($\Delta E_a = 20.8\text{ kcal mol}^{-1}$), making them uncompetitive in the atmosphere. Alternatively, S55-x can react with other RO_2 radicals forming an alkoxy radical S56, followed by decomposition into an alkyl radical S57 via the breakage of C_4-C_5 bond ($\Delta E_a = 2.0\text{ kcal mol}^{-1}$), or fragmentation into an alkyl radical S61 through the cleavage of C_3-C_4 bond ($\Delta E_a = 4.5\text{ kcal mol}^{-1}$). The aforementioned results reveal that the formation of S57 is energetically favorable, which is consistent with the conclusion derived from the unimolecular decomposition of S45 that the breakage of C_4-C_5 bond is feasible. Next, S57 dissociates

tion closed-shell products S47 and S51, with the fractional yields of 26.3 % and 0.3 %, respectively. As a result, the major closed-shell products are 1st-ROOH (S4), 2nd-ROOH (S6), S10-2, S13 and S47 in the multi-generation \bullet OH oxidation of styrene in the low- NO_x conditions.

In the high- NO_x conditions, the fractional yield of the first generation closed-shell product 1st-RONO₂ (S5) formed from the reaction $\text{S2-1-x} + \text{NO}$ is predicted to be 26.5 %, as shown in Fig. S23. As the \bullet OH oxidation reactions proceed, 1st-RONO₂ (S5) can be initially transformed into the peroxy radical P_{S5-add3-a-2}, followed by reaction with NO to form the second generation closed-shell product 2nd-RONO₂ (S26) and an alkoxy radical P_{S5-add3-a-3}, with the fractional yields of 4.8 % and 11.2 %, respectively. The decomposition of P_{S5-add3-a-3} undergoes via two distinct pathways. One is the C₅–C₆ bond cleavage, leading to an alkyl radical S27 with the fractional yield of 7.8 %. The other is the cyclization, resulting in an alkyl radical S35 with the fractional yield of 3.4 %. The resulting S27 and S35 undergo multiple oxidation steps, finally leading to the formation of the second generation closed-shell products S30-2, S33 and S40-1, with the fractional yields of 6.0 %, 1.8 %, and 1.7 %, respectively. 2nd-RONO₂ (S26) can be further oxidized to yield the third generation closed-shell products S58 and S62, with the fractional yields of 2.6 % and 0.03 %, respectively. In summary, the major closed-shell products are 1st-RONO₂ (S5), 2nd-RONO₂ (S26), S30-2 and S58 in the multi-generation \bullet OH oxidation of styrene in the high- NO_x conditions.

3.4 Volatility classes

The volatility classes for various organic compounds are based on their saturation concentration, as proposed by Donahue et al. (2012). The saturated vapour pressure (P^0) and saturated concentration (c^0) of styrene and its multi-generation \bullet OH oxidation products are predicted by using the SIMPOL.1 method (Pankow et al., 2008). As shown in Table S8 in the Supplement, the P^0 and c^0 of the first generation closed-shell product benzaldehyde (C₇H₆O) are 7.62×10^{-4} atm and 2.89×10^6 $\mu\text{g m}^{-3}$, respectively, which are 3–4 orders of magnitude greater than those of S4 (C₈H₁₀O₃, $P^0 = 1.43 \times 10^{-7}$ atm and $c^0 = 8.89 \times 10^2$ $\mu\text{g m}^{-3}$) and S5 (C₈H₉NO₃, $P^0 = 2.54 \times 10^{-7}$ atm and $c^0 = 1.87 \times 10^3$ $\mu\text{g m}^{-3}$). Based on the values of c^0 , benzaldehyde is classified as the volatile organic compounds (VOCs), whereas S4 and S5 are classified as the intermediate volatility organic compounds (IVOCs). These first generation closed-shell products exist exclusively in the gas phase under atmospheric conditions (Bianchi et al., 2019).

For the second generation closed-shell products, S6 (C₈H₁₂O₈, $c^0 = 4.50 \times 10^{-2}$ $\mu\text{g m}^{-3}$) and S26 (C₈H₁₀N₂O₁₀, $c^0 = 0.18$ $\mu\text{g m}^{-3}$) formed from the bimolecular reactions with HO₂ radicals and NO are classified as the low volatility organic compounds (LVOCs). Similarly, S13 (C₈H₁₀O₈,

$c^0 = 2.97 \times 10^{-2}$ $\mu\text{g m}^{-3}$) and S33 (C₈H₁₀O₈, $c^0 = 2.97 \times 10^{-2}$ $\mu\text{g m}^{-3}$), formed through the ring-opening and subsequent intramolecular H-shift reactions of P_{S4-add3-a-3} and P_{S5-add3-a-3}, respectively, are also classified as LVOCs, which can condense onto the existing large particles (Bianchi et al., 2019). The c^0 values of the remaining closed-shell products are significantly greater than those of the aforementioned four products, for example, the c^0 values of S20 (C₆H₈O₆) and S40-1 (C₆H₇NO₇), formed by the cyclization and decomposition reactions of P_{S4-add3-a-3} and P_{S5-add3-a-3}, are 42.21 and 75.86 $\mu\text{g m}^{-3}$, respectively, classifying them as the semivolatile organic compounds (SVOC).

For the third generation closed-shell products, the c^0 values of S47 (C₈H₁₂O₉, $c^0 = 2.68 \times 10^{-4}$ $\mu\text{g m}^{-3}$) and S51 (C₈H₁₀O₁₀, $c^0 = 1.58 \times 10^{-4}$ $\mu\text{g m}^{-3}$), formed through the O₂-addition and subsequent decomposition reactions of P_{S6-add3}, are about two orders of magnitude lower than those of the second generation closed-shell products S6 and S13, despite being classified as LVOCs. Similarly, S58 (C₈H₁₁NO₁₀, $c^0 = 5.37 \times 10^{-4}$ $\mu\text{g m}^{-3}$) and S62 (C₈H₁₀N₂O₁₂, $c^0 = 6.18 \times 10^{-4}$ $\mu\text{g m}^{-3}$), formed via the O₂-addition and subsequent decomposition reactions of P_{S26-add3}, exhibit lower c^0 values compared to the second generation closed-shell products S26 and S33. The aforementioned results reveal that the volatility of the multi-generation \bullet OH oxidation products significantly decreases with increasing the number of \bullet OH oxidation steps. As the oxidation reactions of the third generation closed-shell products proceed further, the formed products may possess sufficiently low volatility to participate in the formation and growth of new aerosol particle.

4 Conclusions and atmospheric implications

The results reveal that the first generation RO₂ radicals, formed from the addition of OH radicals to the C_β-site of a vinyl group in styrene followed by O₂-addition, can proceed intramolecular H-shifts to generate various alkyl and alkoxy radicals. The rate coefficient $k_{\text{MC-TST}}$ is calculated to be 1.6×10^{-4} s⁻¹. Among the competing H-shift pathways, the hydrogen atom transfer from the –OH group to the terminal oxygen atom of the –OO group has the lowest barrier. The resulting alkoxy radical can further decompose into benzaldehyde through the successive elimination of HCHO and an OH radical. The 1,5-H shift reaction occurring at the –OH group is the rate-determining step in the formation of benzaldehyde. Alternatively, the first generation RO₂ radicals can proceed bimolecular reactions with HO₂ radicals and NO, leading to the formation of the first generation closed-shell C7- and C8-products 1st-ROOH (C₈H₁₀O₃), benzaldehyde (C₇H₆O), and 1st-RONO₂ (C₈H₉NO₃).

For the second generation \bullet OH oxidation, OH-addition reaction occurring at the *ortho*-site of 1st-ROOH and 1st-RONO₂ has a significant dominance. This is consistent with

the analogous reaction systems, toluene + $\bullet\text{OH}$ and phenol + $\bullet\text{OH}$, in which *ortho*-OH-addition reaction is energetically favorable (Wu et al., 2020; Xu and Wang, 2013). The resulting alkyl radicals may undergo two O_2 -addition steps and a cyclization process to form BPR, which can react with HO_2 radicals and NO to yield the corresponding BAR, and the second generation closed-shell C8-product 2nd-ROOH ($\text{C}_8\text{H}_{12}\text{O}_8$) and 2nd-RONO₂ ($\text{C}_8\text{H}_{10}\text{N}_2\text{O}_{10}$), with the fractional yields of 41.4 % and 4.8 %. The unimolecular decomposition of BAR formed in the reaction 1st-ROOH + $\bullet\text{OH}$ includes two distinct pathways: (1) ring-opening and followed by decomposition, yielding the multifunctional products S10-2 ($\text{C}_4\text{H}_6\text{O}_5$) and S13 ($\text{C}_8\text{H}_{10}\text{O}_8$) with the fractional yields of 5.6 % and 2.2 %, respectively; or (2) cyclization and followed by dissociation, generating the closed-shell C6-product S23 ($\text{C}_6\text{H}_6\text{O}_5$) with the fractional yield of 1.3 %. The major products formed from the unimolecular decomposition of BAR in the reaction 1st-RONO₂ + $\bullet\text{OH}$ are the multifunctional products S30-2 ($\text{C}_4\text{H}_5\text{NO}_6$), S33 ($\text{C}_8\text{H}_{10}\text{O}_8$) and S40-1 ($\text{C}_6\text{H}_7\text{NO}_7$), with the fractional yields of 6.0 %, 1.8 % and 1.7 %, respectively.

For the third generation $\bullet\text{OH}$ oxidation, the addition of OH radicals to the C=C bond in 2nd-ROOH and 2nd-RONO₂ is the dominant pathway. The resulting alkyl radicals can proceed a series of reactions to produce the alkoxy radicals, which subsequently decompose into an OH radical byproduct and a closed-shell C₈-product S47 ($\text{C}_8\text{H}_{12}\text{O}_9$), identified as the favorable pathway in the reaction 2nd-ROOH + $\bullet\text{OH}$. S47 contains a -OOH, a peroxide bridge, two carbonyls, and three hydroxy groups. The major product formed in the reaction 2nd-RONO₂ + $\bullet\text{OH}$ is a closed-shell C₈-product S58 ($\text{C}_8\text{H}_{11}\text{NO}_{10}$), which contain a -NO₃, a peroxide bridge, two carbonyls, and three hydroxy groups. The fractional yields of S47 and S58 are 26.3 % and 2.6 %, respectively. The volatility of the oxidation products significantly decreases with increasing the number of $\bullet\text{OH}$ oxidation steps in the multi-generation $\bullet\text{OH}$ oxidation of styrene.

In the laboratory chamber experiments, the structures of some specific oxidation products remain uncharacterized but are merely inferred from the exact mass and fragmentation data. Using high-level quantum chemistry methods, we identify the molecular structures of multifunctional products and elucidate their formation pathways in the multi-generation $\bullet\text{OH}$ oxidation of styrene. The mechanistic insights derived from this work are broadly applicable to the photooxidation of structurally analogous aromatics. Furthermore, we quantify the yields of multifunctional products and demonstrate that their volatility decreases significantly with increasing the number of $\bullet\text{OH}$ oxidation steps. The resulting multifunctional products may undergo a series of oxidation reactions to form low volatility compounds, thereby contributing to the formation and growth of new aerosol particle. In the future, more detailed experimental and theoretical studies need to be conducted to identify the molecular structures and formation pathways of multifunctional products formed through

the photooxidation of other aromatics under both low and high-NO_x conditions. These studies will facilitate a more accurate characterization of the chemical composition and formation yields of aromatic SOA, and thereby help narrow the gap between the measured and modeled SOA concentrations in urban environments.

Data availability. Datasets are accessible by contacting the corresponding author, Yu Huang, (huangyu@ieecas.cn).

Supplement. Tables S1 and S3 list the energy barriers of all the elementary reactions involved in the addition of OH radicals to styrene and 1st-ROOH (S4) predicted at different levels. Tables S2, S4 and S6 list the relative electronic energy, free energy and Boltzmann population of different conformers involved in S2-1-x, S8-x and S28-x. Tables S5 and S7 list the MC-TST rate coefficients for the intramolecular H-shift reactions of S8-x and S28-x. Table S8 summaries the saturated vapour pressure and saturated concentrations of styrene and its multiple generation $\bullet\text{OH}$ oxidation closed-shell products. Figures S1–S3 display the PESs for the unimolecular reactions of S2-2-x, S2-3-x and S2-4-x. Figure S4 shows the global minimum structures of 1st-ROOH(S4) and 1st-RONO₂(S5). Figure S5 depicts the geometric parameters of toluene and 1st-ROOH (S4) and the NPA atomic charges of all the carbon atoms. Figures S6 and S11 show the PESs for the addition reactions $\text{P}_{\text{S4-add1}} + \text{O}_2$ and $\text{P}_{\text{S5-add1}} + \text{O}_2$. Figures S7 and S12 present the lowest energy conformers of third generation peroxy radicals $\text{P}_{\text{S4-add3-a-2}}$ and $\text{P}_{\text{S5-add3-a-2}}$. Figures S8–S10 depict the PESs for the intramolecular hydrogen transfer reactions of S8-x, S12-x and S16-x. Figures S13–S15 depict the PESs for the intramolecular hydrogen transfer reactions of S28-x, S32-x and S36-x. Figures S16–18 show the PESs for the OH-initiated oxidation of 2nd-ROOH (S6) and unimolecular decomposition of $\text{P}_{\text{S6-add3}}$. Figures S19–S21 show the PESs for the OH-initiated oxidation of 2nd-RONO₂ (S26) and unimolecular decomposition of $\text{P}_{\text{S26-add3}}$. Figures S22 and S23 show the overall reaction mechanism of the multi-generation $\bullet\text{OH}$ oxidation of styrene in the low- and high-NO_x conditions. The supplement related to this article is available online at <https://doi.org/10.5194/acp-26-4823-2026-supplement>.

Author contributions. LC and YH conceptualized the study. LC conducted quantum chemical calculation. YX and ZJ analyzed the data. LC conducted the volatility estimation. All authors discussed the results and commented on the manuscript.

Competing interests. The contact author has declared that none of the authors has any competing interests.

Disclaimer. Publisher's note: Copernicus Publications remains neutral with regard to jurisdictional claims made in the text, published maps, institutional affiliations, or any other geographical representation in this paper. The authors bear the ultimate responsibility for providing appropriate place names. Views expressed in the

text are those of the authors and do not necessarily reflect the views of the publisher.

Financial support. This study was supported by the National Natural Science Foundation of China (grant no. 42175134) and the Youth Innovation Promotion Association of the Chinese Academy of Sciences (grant no. 2022415).

Review statement. This paper was edited by Arthur Chan and reviewed by two anonymous referees.

References

- Alecu, I. M., Zheng, J., Zhao, Y., and Truhlar, D. G.: Computational thermochemistry: scale factor databases and scale factors for vibrational frequencies obtained from electronic model chemistries, *J. Chem. Theory Comput.*, 6, 2872–2887, <https://doi.org/10.1021/ct100326h>, 2010.
- Arathala, P. and Musah, R. A.: Atmospheric chemistry of chloroprene initiated by OH radicals: combined Ab initio/DFT calculations and kinetics analysis, *J. Phys. Chem. A*, 128, 8983–8995, <https://doi.org/10.1021/acs.jpca.4c05428>, 2024.
- Atkinson, R. and Arey, J.: Atmospheric degradation of volatile organic compounds, *Chem. Rev.*, 103, 4605–4638, <https://doi.org/10.1021/cr0206420>, 2003.
- Bianchi, F., Kurtén, T., Riva, M., Mohr, C., Rissanen, M. P., Roldin, P., Berndt, T., Crounse, J. D., Wennberg, P. O., Mentel, T. F., Wildt, J., Junninen, H., Jokinen, T., Kulmala, M., Worsnop, D. R., Thornton, J. A., Donahue, N., Kjaergaard, H. G., and Ehn, M.: Highly oxygenated organic molecules (HOM) from gas-phase autoxidation involving peroxy radicals: a key contributor to atmospheric aerosol, *Chem. Rev.*, 119, 3472–3509, <https://doi.org/10.1021/acs.chemrev.8b00395>, 2019.
- Bloss, C., Wagner, V., Jenkin, M. E., Volkamer, R., Bloss, W. J., Lee, J. D., Heard, D. E., Wirtz, K., Martin-Reviejo, M., Rea, G., Wenger, J. C., and Pilling, M. J.: Development of a detailed chemical mechanism (MCMv3.1) for the atmospheric oxidation of aromatic hydrocarbons, *Atmos. Chem. Phys.*, 5, 641–664, <https://doi.org/10.5194/acp-5-641-2005>, 2005.
- Boyd, A. A., Flaud, P. M., Daugey, N., and Lesclaux, R.: Rate constants for $\text{RO}_2 + \text{HO}_2$ reactions measured under a large excess of HO_2 , *J. Phys. Chem. A*, 107, 818–821, <https://doi.org/10.1021/jp026581r>, 2003.
- Cabrera-Perez, D., Taraborrelli, D., Sander, R., and Pozzer, A.: Global atmospheric budget of simple monocyclic aromatic compounds, *Atmos. Chem. Phys.*, 16, 6931–6947, <https://doi.org/10.5194/acp-16-6931-2016>, 2016.
- Canneaux, S., Bohr, F., and Henon, E.: KiSThelP: a program to predict thermodynamic properties and rate constants from quantum chemistry results, *J. Comput. Chem.*, 35, 82–93, <https://doi.org/10.1002/jcc.23470>, 2013.
- Chen, L., Huang, Y., Xue, Y., Jia, Z., and Wang, W.: Atmospheric oxidation of 1-butene initiated by OH radical: Implications for ozone and nitrous acid formations, *Atmos. Environ.*, 244, 118010–118021, <https://doi.org/10.1016/j.atmosenv.2020.118010>, 2021.
- Cho, J., Roueintan, M., and Li, Z.: Kinetic and dynamic investigations of OH reaction with styrene, *J. Phys. Chem. A*, 118, 9460–9470, <https://doi.org/10.1021/jp501380j>, 2014.
- Donahue, N. M., Kroll, J. H., Pandis, S. N., and Robinson, A. L.: A two-dimensional volatility basis set – Part 2: Diagnostics of organic-aerosol evolution, *Atmos. Chem. Phys.*, 12, 615–634, <https://doi.org/10.5194/acp-12-615-2012>, 2012.
- Eckart, C.: The penetration of a potential barrier by electrons, *Phys. Rev.*, 35, 1303–1309, <https://doi.org/10.1103/PhysRev.35.1303>, 1930.
- Environmental Protection Agency (EPA): Clean Air Act: Title I-Air Pollution Prevention and Control. U.S., ISBN: 978-0314835024, 1990.
- Fernández-Ramos, A., Ellingson, B. A., Meana-Pañeda, R., Marques, J. M. C., and Truhlar, D. G.: Symmetry numbers and chemical reaction rates, *Theor. Chem. Acc.*, 118, 813–826, <https://doi.org/10.1007/s00214-007-0328-0>, 2007.
- Forstner, H. J. L., Flagan, R. C., and Seinfeld, J. H.: Secondary organic aerosol from the photooxidation of aromatic hydrocarbons: molecular composition, *Environ. Sci. Technol.*, 31, 1345–1358, <https://doi.org/10.1021/es9605376>, 1997.
- Frisch, M. J., Trucks, G. W., Schlegel, H. B., Scuseria, G. E., Robb, M. A., Cheeseman, J. R., Scalmani, G., Barone, V., Petersson, G. A., Nakatsuji, H., Li, X., Caricato, M., Marenich, A. V., Bloino, J., Janesko, B. G., Gomperts, R., Mennucci, B., Hratchian, H. P., Ortiz, J. V., Izmaylov, A. F., Sonnenberg, J. L., Williams-Young, D., Ding, F., Lipparini, F., Egidi, F., Gogings, J., Peng, B., Petrone, A., Henderson, T., Ranasinghe, D., Zakrzewski, V. G., Gao, J., Rega, N., Zheng, G., Liang, W., Hada, M., Ehara, M., Toyota, K., Fukuda, R., Hasegawa, J., Ishida, M., Nakajima, T., Honda, Y., Kitao, O., Nakai, H., Vreven, T., Throssell, K., Montgomery, J. A., Peralta, J. J. E., Ogliaro, F., Bearpark, M. J., Heyd, J. J., Brothers, E. N., Kudin, K. N., Staroverov, V. N., Keith, T. A., Kobayashi, R., Normand, J., Raghavachari, K., Rendell, A. P., Burant, J. C., Iyengar, S. S., Tomasi, J., Cossi, M., Millam, J. M., Klene, M., Adamo, C., Cammi, R., Ochterski, J. W., Martin, R. L., Morokuma, K., Farkas, O., Foresman, J. B., and Fox, D. J.: Gaussian 16, Revision B.01, Gaussian, Inc., Wallingford CT, <https://www.gaussian.com> (last access: 20 June 2025), 2016.
- Fu, Z., Xie, H. B., Elm, J., Guo, X., Fu, Z., and Chen, J.: Formation of low-volatile products and unexpected high formaldehyde yield from the atmospheric oxidation of methylsiloxanes, *Environ. Sci. Technol.*, 54, 7136–7145, <https://doi.org/10.1021/acs.est.0c01090>, 2020.
- Fu, Z., Ma, F., Liu, Y., Yan, C., Huang, D., Chen, J., Elm, J., Li, Y., Ding, A., Pichelstorfer, L., Xie, H. B., Nie, W., Francisco, J. S., and Zhou, P.: An overlooked oxidation mechanism of toluene: computational predictions and experimental validations, *Chem. Sci.*, 14, 13050–13059, <https://doi.org/10.1039/D3SC03638C>, 2023.
- Fu, Z., Guo, S., Xie, H. B., Zhou, P., Boy, M., Yao, M., and Hu, M.: A near-explicit reaction mechanism of chlorine-initiated limonene: implications for health risks associated with the concurrent use of cleaning agents and disinfectants, *Environ. Sci. Technol.*, 58, 19762–19773, <https://doi.org/10.1021/acs.est.4c04388>, 2024.

- Fukui, K.: The path of chemical reactions – the IRC approach, *Accounts Chem. Res.*, 14, 363–368, <https://doi.org/10.1021/ar00072a001>, 1981.
- Garmash, O., Rissanen, M. P., Pullinen, I., Schmitt, S., Kausiala, O., Tillmann, R., Zhao, D., Percival, C., Bannan, T. J., Priestley, M., Hallquist, Å. M., Kleist, E., Kiendler-Scharr, A., Hallquist, M., Berndt, T., McFiggans, G., Wildt, J., Mentel, T. F., and Ehn, M.: Multi-generation OH oxidation as a source for highly oxygenated organic molecules from aromatics, *Atmos. Chem. Phys.*, 20, 515–537, <https://doi.org/10.5194/acp-20-515-2020>, 2020.
- Gilbert, R. G. and Smith, S. C.: *Theory of unimolecular and recombination reactions*, Blackwell Scientific, Carlton, Australia, ISBN: 978-0632027491, 1990.
- Glowacki, D. R., Liang, C. H., Morley, C., Pilling, M. J., and Robertson, S. H.: MESMER: an open-source master equation solver for multi-energy well reactions, *J. Phys. Chem. A*, 116, 9545–9560, <https://doi.org/10.1021/jp3051033>, 2012.
- Holbrook, K. A., Pilling, M. J., Robertson, S. H., and Robinson, P. J.: *Unimolecular reactions*, 2nd edn., Wiley, New York, ISBN: 978-0471922681, 1996.
- Huang, Y., Su, T., Wang, L., Wang, N., Xue, Y., Dai, W., Lee, S. C., Cao, J., and Ho, S. S. H.: Evaluation and characterization of volatile air toxics indoors in a heavy polluted city of north-western China in wintertime, *Sci. Total Environ.*, 662, 470–480, <https://doi.org/10.1016/j.scitotenv.2019.01.250>, 2019.
- Luga, C., Galano, A., and Vivier-Bunge, A.: Theoretical investigation of the OH-initiated oxidation of benzaldehyde in the troposphere, *Chem. Phys. Chem.*, 9, 1453–1459, <https://doi.org/10.1002/cphc.200800144>, 2008.
- Iyer, S., Kumar, A., Savolainen, A., Barua, S., Daub, C., Pichelstorfer, L., Roldin, P., Garmash, O., Seal, P., Kurtén, T., and Rissanen, M.: Molecular rearrangement of bicyclic peroxy radicals is a key route to aerosol from aromatics, *Nat. Commun.*, 14, 4984–4991, <https://doi.org/10.1038/s41467-023-40675-2>, 2023.
- Ji, Y., Zhao, J., Terazono, H., Misawa, K., Levitt, N. P., Li, Y., Lin, Y., Peng, J., Wang, Y., Duan, L., Pan, B., Zhang, F., Feng, X., An, T., Marrero-Ortiz, W., Secret, J., Zhang, A. L., Shibuya, K., Molina, M. J., and Zhang, R.: Reassessing the atmospheric oxidation mechanism of toluene, *P. Natl. Acad. Sci. USA*, 114, 8169–8174, <https://doi.org/10.1073/pnas.1705463114>, 2017.
- Koppmann, R.: *Volatile organic compounds in the atmosphere*, John Wiley & Sons, ISBN: 978-1405131155, 2008.
- Li, M., Zhang, Q., Zheng, B., Tong, D., Lei, Y., Liu, F., Hong, C., Kang, S., Yan, L., Zhang, Y., Bo, Y., Su, H., Cheng, Y., and He, K.: Persistent growth of anthropogenic non-methane volatile organic compound (NMVOC) emissions in China during 1990–2017: drivers, speciation and ozone formation potential, *Atmos. Chem. Phys.*, 19, 8897–8913, <https://doi.org/10.5194/acp-19-8897-2019>, 2019.
- Lu, T.: Molclus program, Version 1.9.3., <http://www.keinsci.com/research/molclus.html> (last access: 21 May 2024), 2019.
- Ma, F., Guo, X., Xia, D., Xie, H. B., Wang, Y., Elm, J., Chen, J., and Niu, J.: Atmospheric chemistry of allylic radicals from isoprene: a successive cyclization-driven autoxidation mechanism, *Environ. Sci. Technol.*, 55, 4399–4409, <https://doi.org/10.1021/acs.est.0c07925>, 2021.
- Møller, K. H., Otkjær, R. V., Hyttinen, N., Kurtén, T., and Kjaergaard, H. G.: Cost-effective implementation of multi-conformer transition state theory for peroxy radical hydrogen shift reactions, *J. Phys. Chem. A*, 120, 10072–10087, <https://doi.org/10.1021/acs.jpca.6b09370>, 2016.
- Møller, K. H., Berndt, T., and Kjaergaard, H. G.: Atmospheric autoxidation of amines, *Environ. Sci. Technol.*, 54, 11087–11099, <https://doi.org/10.1021/acs.est.0c03937>, 2020.
- Molteni, U., Bianchi, F., Klein, F., El Haddad, I., Frege, C., Rossi, M. J., Dommen, J., and Baltensperger, U.: Formation of highly oxygenated organic molecules from aromatic compounds, *Atmos. Chem. Phys.*, 18, 1909–1921, <https://doi.org/10.5194/acp-18-1909-2018>, 2018.
- Neese, F.: Software update: the ORCA program system – version 6.0, *Wires Comput. Mol. Sci.*, 15, e70019, <https://doi.org/10.1002/wcms.70019>, 2025.
- Nie, W., Yan, C., Huang, D. D., Wang, Z., Liu, Y., Qiao, X., Guo, Y., Tian, L., Zheng, P., Xu, Z., Li, Y., Xu, Z., Qi, X., Sun, P., Wang, J., Zheng, F., Li, X., Yin, R., Dallenbach, K. R., Bianchi, F., Petäjä, T., Zhang, Y., Wang, M., Schervish, M., Wang, S., Qiao, L., Wang, Q., Zhou, M., Wang, H., Yu, C., Yao, D., Guo, H., Ye, P., Lee, S., Li, Y. J., Liu, Y., Chi, X., Kerminen, V. M., Ehn, M., Donahue, N. M., Wang, T., Huang, C., Kulmala, M., Worsnop, D., Jiang, J., and Ding, A.: Secondary organic aerosol formed by condensing anthropogenic vapours over China’s megacities, *Nat. Geosci.*, 15, 255–261, <https://doi.org/10.1038/s41561-022-00922-5>, 2022.
- Orlando, J. J. and Tyndall, G. S.: Laboratory studies of organic peroxy radical chemistry: an overview with emphasis on recent issues of atmospheric significance, *Chem. Soc. Rev.*, 41, 6294–6317, <https://doi.org/10.1039/C2CS35166H>, 2012.
- Pankow, J. F. and Asher, W. E.: SIMPOL.1: SIMPOL.1: a simple group contribution method for predicting vapor pressures and enthalpies of vaporization of multifunctional organic compounds, *Atmos. Chem. Phys.*, 8, 2773–2796, <https://doi.org/10.5194/acp-8-2773-2008>, 2008.
- Pasik, D., Frandsen, B. N., Meder, M., Iyer, S., Kurtén, T., and Myllys, N.: Gas-phase oxidation of atmospherically relevant unsaturated hydrocarbons by acyl peroxy radicals, *J. Am. Chem. Soc.*, 146, 13427–13437, <https://doi.org/10.1021/jacs.4c02523>, 2024.
- Sebban, N., Bozzelli, J. W., and Bockhorn, H.: Thermochemistry and reaction paths in the oxidation reaction of benzoyl radical: $C_6H_5C(=O)$, *J. Phys. Chem. A*, 115, 11897–11914, <https://doi.org/10.1021/jp2078067>, 2011.
- Shen, H., Vereecken, L., Kang, S., Pullinen, I., Fuchs, H., Zhao, D., and Mentel, T. F.: Unexpected significance of a minor reaction pathway in daytime formation of biogenic highly oxygenated organic compounds, *Sci. Adv.*, 8, eabp8702, <https://doi.org/10.1126/sciadv.abp8702>, 2022.
- Sun, J., Wu, F., Hu, B., Tang, G., Zhang, J., and Wang, Y.: VOC characteristics, emissions and contributions to SOA formation during hazy episodes, *Atmos. Environ.*, 141, 560–570, <https://doi.org/10.1016/j.atmosenv.2016.06.060>, 2016.
- Tajuelo, M., Rodríguez, D., Baeza-Romero, M. T., Díaz-de-Mera, Y., Aranda, A., and Rodríguez, A.: Secondary organic aerosol formation from styrene photolysis and photooxidation with hydroxyl radicals, *Chemosphere*, 231, 276–286, <https://doi.org/10.1016/j.chemosphere.2019.05.136>, 2019a.
- Tajuelo, M., Rodríguez, A., Baeza-Romero, M. T., Aranda, A., Díaz-de-Mera, Y., and Rodríguez, D.: Secondary organic aerosol formation from α -methylstyrene atmospheric degra-

- dation: Role of NO_x level, relative humidity and inorganic seed aerosol, *Atmos. Res.*, 230, 104631–104640, <https://doi.org/10.1016/j.atmosres.2019.104631>, 2019b.
- Tajuelo, M., Bravo, I., Rodríguez, A., Aranda, A., Díaz-de-Mera, Y., and Rodríguez, D.: Atmospheric sink of styrene, α -methylstyrene, trans- β -methylstyrene and indene: Rate constants and mechanisms of Cl atom-initiated degradation, *Atmos. Environ.*, 200, 78–89, <https://doi.org/10.1016/j.atmosenv.2018.11.059>, 2019c.
- Vereecken, L., Glowacki, D. R., and Pilling, M. J.: Theoretical chemical kinetics in tropospheric chemistry: methodologies and applications, *Chem. Rev.*, 115, 4063–4114, <https://doi.org/10.1021/cr500488p>, 2015.
- Wang, H., Ji, Y., Gao, Y., Li, G., and An, T.: Theoretical model on the formation possibility of secondary organic aerosol from OH initiated oxidation reaction of styrene in the presence of O_2/NO , *Atmos. Environ.*, 101, 1–9, <https://doi.org/10.1016/j.atmosenv.2014.10.042>, 2015.
- Wang, L., Wu, R., and Xu, C.: Atmospheric oxidation mechanism of benzene. Fates of alkoxy radical intermediates and revised mechanism, *J. Phys. Chem. A*, 117, 14163–14168, <https://doi.org/10.1021/jp4101762>, 2013.
- Wang, M., Chen, D., Xiao, M., Ye, Q., Stolzenburg, D., Hofbauer, V., Ye, P., Vogel, A. L., Mauldin, R. L., Amorim, A., Baccharini, A., Baumgartner, B., Brilke, S., Dada, L., Dias, A., Duplissy, J., Finkenzeller, H., Garmash, O., He, X. C., Hoyle, C. R., Kim, C., Kvashnin, A., Lehtipalo, K., Fischer, L., Molteni, U., Petäjä, T., Pospisilova, V., Quéléver, L. L. J., Rissanen, M., Simon, M., Tauber, C., Tomé, A., Wagner, A. C., Weitz, L., Volkamer, R., Winkler, P. M., Kirkby, J., Worsnop, D. R., Kulmala, M., Baltensperger, U., Dommen, J., El-Haddad, I., and Donahue, N. M.: Photo-oxidation of aromatic hydrocarbons produces low-volatility organic compounds, *Environ. Sci. Technol.*, 54, 7911–7921, <https://doi.org/10.1021/acs.est.0c02100>, 2020a.
- Wang, S. and Li, H.: NO_3 -initiated gas-phase formation of nitrated phenolic compounds in polluted atmosphere, *Environ. Sci. Technol.*, 55, 2899–2907, <https://doi.org/10.1021/acs.est.0c08041>, 2021.
- Wang, S., Wu, R., Berndt, T., Ehn, M., and Wang, L.: Formation of highly oxidized radicals and multifunctional products from the atmospheric oxidation of alkylbenzene, *Environ. Sci. Technol.*, 51, 8442–8449, <https://doi.org/10.1021/acs.est.7b02374>, 2017.
- Wang, S., Newland, M. J., Deng, W., Rickard, A. R., Hamilton, J. F., Muñoz, A., Ródenas, M., Vázquez, M. M., Wang, L., and Wang, X.: Aromatic photo-oxidation, a new source of atmospheric acidity, *Environ. Sci. Technol.*, 54, 7798–7806, <https://doi.org/10.1021/acs.est.0c00526>, 2020b.
- Wu, R., Pan, S., Li, Y., and Wang, L.: Atmospheric oxidation mechanism of toluene, *J. Phys. Chem. A*, 118, 4533–4547, <https://doi.org/10.1021/jp500077f>, 2014.
- Wu, X., Huang, C., Niu, S., and Zhang, F.: New theoretical insights into the reaction kinetics of toluene and hydroxyl radicals, *Phys. Chem. Chem. Phys.*, 22, 22279–22288, <https://doi.org/10.1039/D0CP02984J>, 2020.
- Wu, X., Hou, Q., Huang, J., Chai, J., and Zhang, F.: Exploring the OH-initiated reactions of styrene in the atmosphere and the role of van der Waals complex, *Chemosphere*, 282, 131004–131012, <https://doi.org/10.1016/j.chemosphere.2021.131004>, 2021.
- Xu, C. and Wang, L.: Atmospheric oxidation mechanism of phenol initiated by OH radical, *J. Phys. Chem. A*, 117, 2358–2364, <https://doi.org/10.1021/jp308856b>, 2013.
- Xu, L., Møller, K. H., Crouse, J. D., Kjaergaard, H. G., and Wennberg, P. O.: New insights into the radical chemistry and product distribution in the OH-initiated oxidation of benzene, *Environ. Sci. Technol.*, 54, 13467–13477, <https://doi.org/10.1021/acs.est.0c04780>, 2020.
- Yan, Y., Cabrera-Perez, D., Lin, J., Pozzer, A., Hu, L., Millet, D. B., Porter, W. C., and Lelieveld, J.: Global tropospheric effects of aromatic chemistry with the SAPRC-11 mechanism implemented in GEOS-Chem version 9-02, *Geosci. Model Dev.*, 12, 111–130, <https://doi.org/10.5194/gmd-12-111-2019>, 2019.
- Yang, F., Deng, F., Pan, Y., Zhang, Y., Tang, C., and Huang, Z.: Kinetics of hydrogen abstraction and addition reactions of 3-hexene by OH radicals, *J. Phys. Chem. A*, 121, 1877–1889, <https://doi.org/10.1021/acs.jpca.6b11499>, 2017.
- Yu, S., Jia, L., Xu, Y., and Pan, Y.: Formation of extremely low-volatility organic compounds from styrene ozonolysis: Implication for nucleation, *Chemosphere*, 305, 135459–135467, <https://doi.org/10.1016/j.chemosphere.2022.135459>, 2022a.
- Yu, S., Jia, L., Xu, Y., and Pan, Y.: Molecular composition of secondary organic aerosol from styrene under different NO_x and humidity conditions, *Atmos. Res.*, 266, 105950–10604, <https://doi.org/10.1016/j.atmosres.2021.105950>, 2022b.
- Zaytsev, A., Koss, A. R., Breitenlechner, M., Krechmer, J. E., Nihil, K. J., Lim, C. Y., Rowe, J. C., Cox, J. L., Moss, J., Roscioli, J. R., Canagaratna, M. R., Worsnop, D. R., Kroll, J. H., and Keutsch, F. N.: Mechanistic study of the formation of ring-retaining and ring-opening products from the oxidation of aromatic compounds under urban atmospheric conditions, *Atmos. Chem. Phys.*, 19, 15117–15129, <https://doi.org/10.5194/acp-19-15117-2019>, 2019.
- Zhang, H., Wang, J., Dong, B., Xu, F., Liu, H., Zhang, Q., Zong, W., and Shi, X.: New mechanism for the participation of aromatic oxidation products in atmospheric nucleation, *Sci. Total Environ.*, 917, 170487–170494, <https://doi.org/10.1016/j.scitotenv.2024.170487>, 2024.
- Zhang, R. M., Truhlar, D. G., and Xu, X.: Kinetics of the toluene reaction with OH radical, *Research*, 2019, 5373785, <https://doi.org/10.34133/2019/5373785>, 2019.
- Zhao, H., Zhang, Y., Zhao, Q., Li, Y., and Huang, Z.: A theoretical study of H-abstractions of benzaldehyde by H, $\text{O}^3(\text{P})$, $^3\text{O}_2$, OH, HO_2 , and CH_3 radicals: Ab initio rate coefficients and their uncertainty quantification, *J. Phys. Chem. A*, 126, 7523–7533, <https://doi.org/10.1021/acs.jpca.2c02384>, 2022.
- Zhao, Y. and Truhlar, D. G.: The M06 suite of density functionals for main group thermochemistry, thermochemical kinetics, non-covalent interactions, excited states, and transition elements: two new functionals and systematic testing of four M06-class functionals and 12 other functionals, *Theor. Chem. Acc.*, 120, 215–241, <https://doi.org/10.1007/s00214-007-0310-x>, 2008.